

Properties and nature of Be stars*

XXIII. Long-term variations and physical properties of κ Dra

S. M. Saad^{1,2}, J. Kubát¹, P. Koubský¹, P. Harmanec^{3,1}, P. Škoda¹, D. Korčáková¹, J. Krtička^{4,1}, M. Šlechta¹,
H. Božić⁵, H. Ak⁶, P. Hadrava¹, and V. Votruba^{4,1}

¹ Astronomický ústav, Akademie věd České republiky, CZ-251 65 Ondřejov, Czech Republic

² National Research Institute of Astronomy and Geophysics, 11421 Helwan, Cairo, Egypt

³ Astronomický ústav UK, V Holešovičkách 2, CZ-180 00 Praha 8, Czech Republic

⁴ Ústav teoretické fyziky a astrofyziky PřF MU, Kotlářská 2, CZ-611 37 Brno, Czech Republic

⁵ Opservatorij Hvar, Geodetski fakultet, Sveučilište Zagreb, 10000 Zagreb, Croatia

⁶ Ankara University, Science Faculty, Astronomy and Space Science Dept., Tandoğan, Ankara, 06100 Turkey

Received 1 September 2003 / Accepted 7 January 2004

Abstract. We present an analysis of new spectroscopic observations of the bright Be star κ Dra obtained at the Ondřejov observatory during 1992 – 2003 and *UBV* photometric observations secured at several observatories. General characteristics and a line identification of the spectrum of κ Dra are obtained in the regions 3730 – 5650 Å and 5850 – 7800 Å by a comparison with the theoretical spectrum. The fundamental stellar parameters have been obtained from a comparison with a grid of NLTE model atmospheres. The best fit was found for $T_{\text{eff}} = 14\,000$ K, $\log g = 3.5$, and $v \sin i = 170$ km s⁻¹. These values together with a Hipparcos parallax lead to a stellar mass $M = 4.8 \pm 0.8 M_{\odot}$ and radius $R = 6.4 \pm 0.5 R_{\odot}$. It is encouraging to see that these values agree well with the expected evolutionary mass and radius for the effective temperature we derived. Long-term variations of κ Dra were analysed using measurements of equivalent widths, central intensities, peak intensities of emission lines and emission peak velocity differences for H α , H β , H γ , H δ , and some helium, silicon, and iron lines. It turned out that the previously reported period of 23 years in the variation of the emission strength is probably a cyclic, not a strictly periodic phenomenon. An attempt to find out a period from all available records of the H β emission strength led to a value of (8044 ± 167) days (22.0 years) but the phase plots show that each cycle has a different shape and length. The maximum strength of the emission lags behind the brightness maximum. This is a behaviour usually observed for long-term changes of Be stars with a positive correlation between the brightness and emission strength. Since there are obviously no published speckle observations of the star, we suggest these should be carried out. They could help to deny or confirm the possibility that the emission episodes are triggered by a periastron passage of a putative binary companion moving in an eccentric orbit with a 8044-d period, as it seems to be the case for some Be binaries. For the moment, the nature and origin of the disk around κ Dra still remains unknown. From the comparison of the electronic spectra obtained at different phases of the long-term cycle and synthetic spectra it appears that there are no detectable changes in the photospheric part of the Balmer lines related to variations in the Balmer emission strength which could be attributed to an extended photosphere corresponding to inner parts of the disk, optically thick in continuum.

Key words. Stars: emission-line, Be – stars: individual: κ Dra – line: profiles

1. Introduction

κ Dra (5 Dra, HD 109387, HR 4787, BD +70°703, MWC 222, HIP 61281) is one of the brightest variable ($V = 3^{\text{m}}75 - 3^{\text{m}}95$) Northern Hemisphere Be stars, for which the bright H α line had already been reported by Campbell (1895). Since that, κ Dra has been a subject of numerous investigations, with

Send offprint requests to: J. Kubát,

e-mail: kubat@sunstel.asu.cas.cz

* Tables 2 to 4 are only available in electronic form at CDS (<http://cdsweb.u-strasbg.fr/cats/J.A+A.txt>) and at <http://www.edpsciences.org>.

many controversial reports on the time scales and character of its variability in various observables. This made it one of the most challenging objects for further studies. A detailed history of its investigation is summarized in papers by Juza et al. (1991, 1994) and Hirata (1995) and need not be repeated here.

The most important results of several more recent studies can be summarized as follows:

1. Periodic variations of the H β emission strength with a period of 23 years, discovered by Jessup (1932), have been confirmed and detected also in photometry and contin-

- uum polarimetry. Their period was improved to 8406 days (23.01 years; Juza et al. 1994).
2. The maximum brightness in the long-term cycle precedes the maximum of the emission strength for a few years (Juza et al. 1994). The maximum of the emission strength coincides with the maximum of continuum polarization (Arsenijević et al. 1994). These facts seem to indicate that the brightening of the object is related to temporarily extended photosphere which can be satisfactorily modelled by rotating model photospheres (Hirata 1995).
 3. α Dra is the primary component of a single-line spectroscopic binary in a circular orbit with an orbital period of $61^{\text{d}}.55$ and a semi-amplitude of $K \sim 7 - 8 \text{ km s}^{-1}$. This orbital radial-velocity (RV hereafter) variations could be detected in virtually all published RVs. They are accompanied by parallel phase-locked V/R variations of the double Balmer emission lines (Juza et al. 1991).
 4. A controversial period of rapid variations of $0^{\text{d}}.890384$ or its various aliases could be found in all available RV data sets, line asymmetry and polarization and its value corresponds well to the expected rotational period of the Be primary (Juza et al. 1991).
 5. The rapid variations in the form of line width and asymmetry and also travelling sub-features, seen in a series of electronic spectra, can best be reconciled with a period of $0^{\text{d}}.545$ (one of the aliases of the $0^{\text{d}}.89$ period according to Juza et al. 1991) and can be interpreted as signatures of nonradial pulsations (Hill 1991).

It is clear that understanding the long-term variability is one of the most important clues to understanding the nature of the still mysterious Be phenomenon. Such a task requires, among other things, a very patient collection of observational data and their careful reduction. Since α Dra has been on our observing program both at Ondřejov (spectroscopy with electronic detectors), and at Hvar, and recently also at Tubitak (*UBV* photometry) for more than a decade, it was deemed useful to publish these unique data sets in extenso, with relevant analyses, to enable further comparisons with current and future theoretical models of the Be phenomenon. We also offer some interpretations and derive improved basic physical properties of the Be star based on detailed comparison with synthetic line profiles over a large range of wavelengths.

2. Observations and data reduction

2.1. Spectroscopy

Electronic spectra of α Dra were secured from June 1992 to April 2003 in the coudé and Cassegrain foci of the Ondřejov 2m telescope. The details of observations are summarized in Table 1.

- Most of the spectra (102) were obtained in the coudé focus with a *Reticon RL-1872F/30* detector at a reciprocal dispersion of 17 \AA/mm ; 93 of them cover the $H\alpha$ region, 6 of them contain $H\beta$ and 3 the $H\gamma$ line.
- Since January 2001 to March 2003, 30 spectra were obtained at the red and blue channels of the fibre-fed echelle

spectrograph *HEROS* (*Heidelberg Extended Range Optical Spectrograph*) attached to the Cassegrain focus. See, e.g., Stahl et al. (1995), Štefl & Rivinius (2000) or Škoda & Šlechta (2002) for more details about *HEROS*.

- 31 spectra were obtained with a *CCD* camera attached to the coudé focus; 24 of them near $H\alpha$, 6 near $H\beta$ and one around $H\gamma$.

A complete reduction of *Reticon* spectra, i.e. wavelength calibration, rectification, and intensity and equivalent-width (W) measurements were all carried out using the program *SPEFO* written by Dr. J. Horn (see Horn et al. 1992, Škoda 1996 for details). All initial reduction of *HEROS* and *CCD* spectra (bias subtraction, flat-fielding and wavelength calibration) were carried out using modified *MIDAS* and *IRAF* packages, respectively. The unrectified, wavelength-calibrated spectra were then exported into *SPEFO* where the rectification and all line parameter measurements were done.

2.2. Photometry

A rich collection of *UBV* photometric observations was obtained at Hvar and Skalnaté Pleso, and complemented by observations collected from the astronomical literature, by Juza et al. (1994). In addition to these observations, we obtained new *UBV* photometry of α Dra at two observatories: 10 observations at Hvar and 47 observations at Tubitak. All these observations were corrected for differential extinction and transformed into a standard *UBV* system (based on the mean values given by Johnson et al. 1966) via non-linear transformation formulæ using *HEC22/VYPAR* photometric software (see Harmanec & Horn 1998 and Harmanec et al. 1994 for the details and copies of the programs). We also extracted 115 H_p photometric observations having photometric flag 0 or 1 from the Hipparcos archive (Perryman et al. 1997) and transformed them into Johnson V magnitude using Harmanec's (1998a) formula. Finally, we read out 96 V magnitude differences from a graph published in a poster paper by Croxall et al. (2001) and shifted them properly to get them on a scale of other data using the nights where this data set overlaps with our calibrated data.

A few comments are relevant:

1. To ensure the best homogeneity of Hvar data, we only used differential photometry of α Dra obtained relative to HR 4687 = HD 107193 for which the following all-sky *UBV* values were adopted on the basis of recent data homogenization $V = 5^{\text{m}}.489$, $B - V = +0^{\text{m}}.038$, $U - B = +0^{\text{m}}.079$. The check star HR 5018 = HD 115612 ($V = 6^{\text{m}}.215$, $B - V = -0^{\text{m}}.056$, $U - B = -0^{\text{m}}.137$) was observed as frequently as the variable.
2. The same comparisons were also used at the 0.4-m reflector at Tubitak.
3. All older Hvar and Skalnaté Pleso *UBV* observations, published by Juza et al. (1994), were also re-reduced relative to the above values for the comparison.

Table 1. The observational journal of α Dra at the Ondřejov Observatory.

Epoch [HJD–2400000]	No. of spectra	Spectrograph	Detector	Resolving power	Spectral range [Å]
48000 – 51714	93	coudé	<i>Reticon</i> RL-1872F/30	10 000	6300 – 6740
49021 – 49026	3	coudé	<i>Reticon</i> RL-1872F/30	10 000	4310 – 4520
49079 – 49116	6	coudé	<i>Reticon</i> RL-1872F/30	10 000	4750 – 4960
52321 – 52321	1	coudé	CCD SITe005 800×2000	10 000	4300 – 4554
52323 – 52323	2	coudé	CCD SITe005 800×2000	10 000	6256 – 6769
51900 – 52727	30	<i>HEROS</i>	CCD EEV 2000×800 CCD EEV 1152×770	20 000 20 000	3450 – 5650 5850 – 8620
52742 – 52754	6	coudé	CCD SITe005 800×2000	10 000	4753 – 5005
52734 – 52754	22	coudé	CCD SITe005 800×2000	10 000	6256 – 6769

3. The optical spectrum of α Dra

The vast majority of the new spectra cover the wavelength region from about 6300 to 6700 Å, which includes the H α line. This spectral region is characterized by a *permanent* presence of emission in H α and Fe II 6456 Å lines, while the lines Si II 6347 Å, Si II 6371 Å, and He I 6678 Å are seen in absorption. In a much wider spectral range 3450 – 8620 Å, covered only by the *HEROS* spectra, the Balmer lines up to H15 as well as some infrared lines are seen.

The general time behaviour documented by the spectral region around H α seems to be confirmed by the rest of the visible spectrum. As usually, the Balmer emission is strongest for H α and decreases toward higher members of the series. A number of Fe II emission lines are present in the whole optical spectrum, whereas both the triplet and singlet He I lines are in absorption. Lines of other ions, like Mg II, C II, O I are all in absorption, with a notable exception of the infrared oxygen triplet O I 7772, 7774, 7775 Å. Note that certain parts of the red and infrared spectrum are strongly contaminated by the telluric absorption lines and bands.

3.1. Comparison with a theoretical spectrum

Determination of basic parameters of stellar atmospheres (the effective temperature T_{eff} and the surface gravity g) is a relatively straightforward procedure for normal, main sequence stars, where simplifying assumptions of local thermodynamic equilibrium (LTE) in a static atmosphere and plane-parallel geometry are fulfilled with a sufficient accuracy.

However, this is not the case for Be stars. The very presence of the emission lines indicates the violation of the assumptions of a plane-parallel geometry and a static atmosphere. Yet, one can try to derive *approximate* values based on standard models, keeping their limited applicability in mind. This should work rather well in circumstances when the star in question is temporarily without any observable signatures of the Be envelope and has a pure absorption spectrum. Indeed, very satisfactory results for two other Be stars, 4 Her (HD 142926) and 60 Cyg (HD 200310), were obtained this way – cf. Koubský et al. (1997) and Koubský et al. (2000), respectively.

Very regrettably, α Dra has never been observed to lose its emission lines completely. Therefore, the following results of

model atmosphere analysis give only an approximate estimate of the effective temperature and gravity.

We calculated a small grid of NLTE plane-parallel hydrogen-helium model atmospheres for all combinations of three values of T_{eff} (13 000 K, 14 000 K, 15 000 K) and $\log g$ (3.0, 3.5, 4.0) using a computer code developed by one of us (see, e.g., Kubát 2003, and references therein). The hydrogen model atom consists of 15 levels of H I and 1 level of H II, the helium model atom consists of 29 levels of He I and 1 level of He II. The atomic data (transition probabilities, photoionization cross-sections, collisional strengths) were the same as described in Kubát (1999). By simple comparison of the observed spectrum of higher Balmer lines to the model one, one finds that the model atmosphere with $T_{\text{eff}} = 14 000$ K and $\log g = 3.5$ leads to quite a satisfactory agreement with the observed spectrum for a rotational velocity of $v \sin i = 170 \text{ km s}^{-1}$.

Rotation of the model spectrum was taken into account in an approximate way using the convolution of the rotation profile with the line profile following Gray (1976).

One can admit that the comparison of the observed and model spectrum should also take into account the radiation of the secondary component of the binary. However, Juza et al. (1991) presented rather convincing arguments that the secondary to α Dra is not a Roche-lobe filling giant but a small compact object with a mass probably smaller than some $0.9 M_{\odot}$. In the whole optical spectrum, the luminosity of such an object would be negligible in comparison to the Be giant and we conclude that one can safely neglect the contribution of the secondary to the observed spectrum in the investigated range of wavelengths. The values of T_{eff} and $\log g$ we found are not too different from those presented by Chauville et al. (2001) in their Table 1, namely $T_{\text{eff}} = 13900$ K and $\log g = 3.84$, based on the BCD classification system (Chalonge & Divan 1952).

The value of $v \sin i$ is in a good agreement with the value 180 km s^{-1} determined by Stoeckley & Buscombe (1987). Higher values of the projection rotational velocity seem to be unrealistic.

The observed and theoretical spectrum is compared in Figures 1 and 2, which correspond to wavelength regions covered by the blue and red channel of the *HEROS* spectrograph, respectively. Both parts of the spectrum were obtained simultaneously at HJD 51924.5409.

One can see that there is a general agreement between the

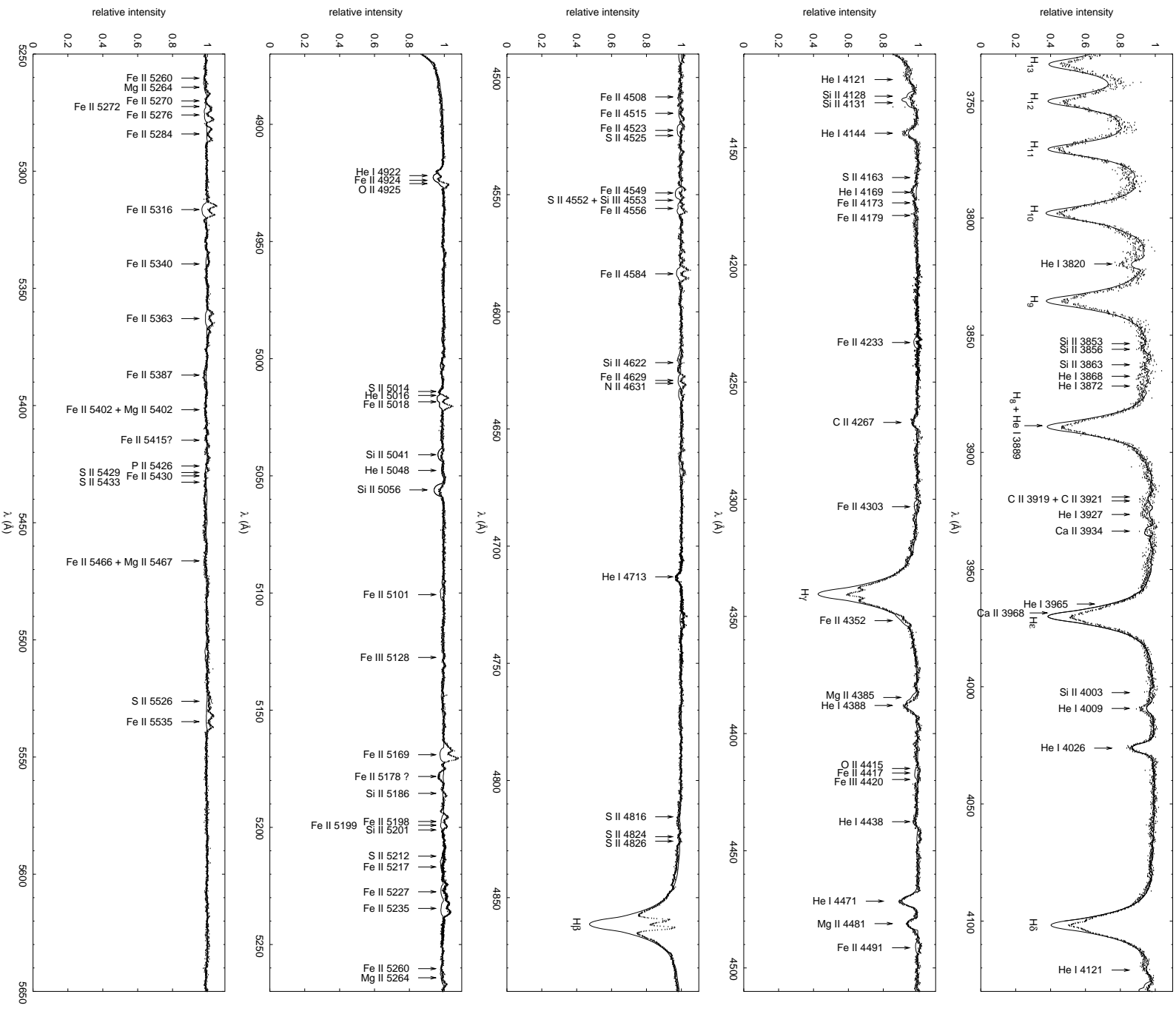


Fig. 1. Line identification and comparison of the spectrum of α Dra obtained using the blue channel of the HEROS spectrograph (dots) and the synthetic NLTE spectrum $T_{\text{eff}} = 14\,000$ K, $\log g = 3.5$ (full line).

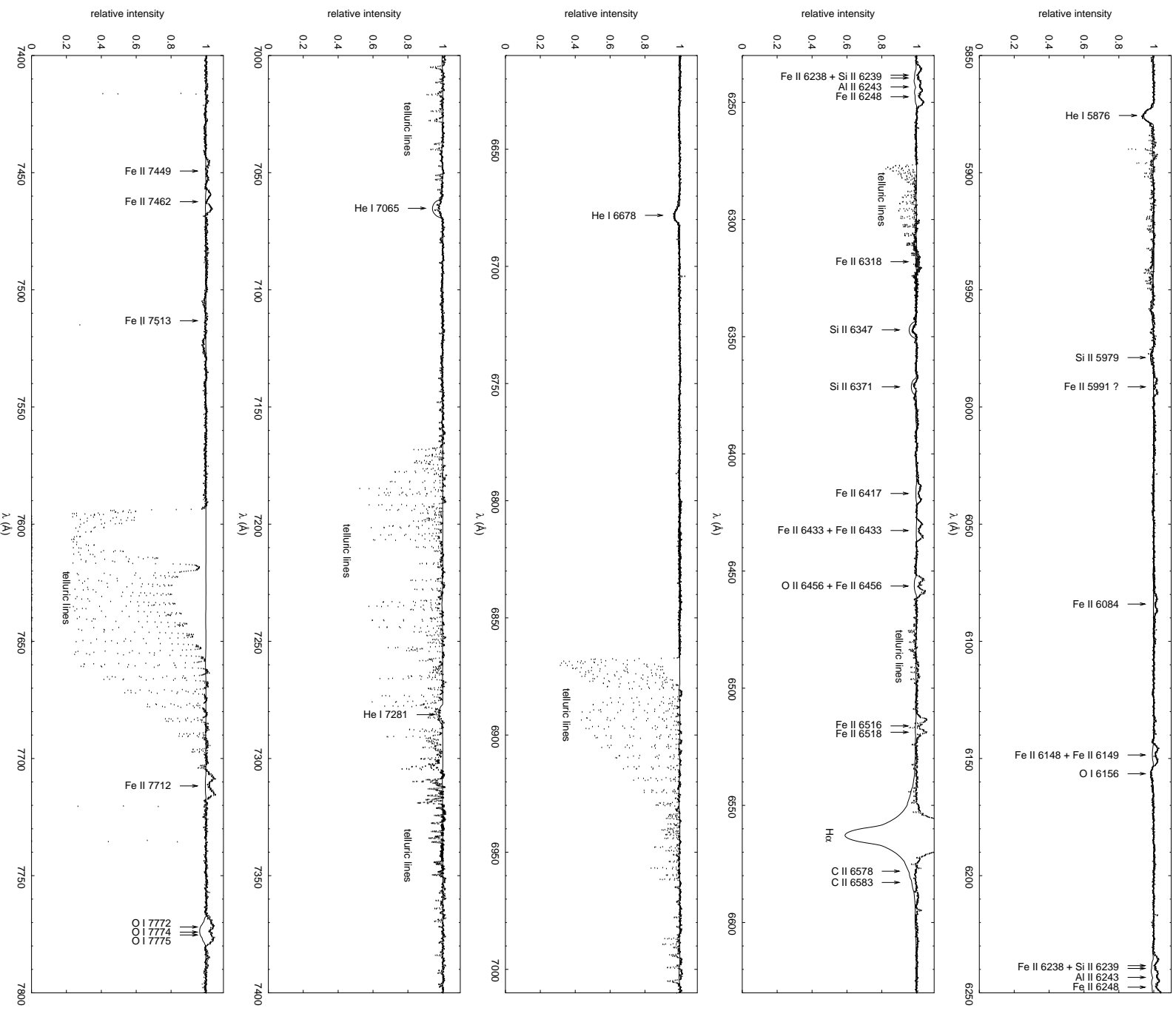


Fig. 2. Line identification and comparison of the spectrum of α Dra obtained using the *HEROS* spectrograph (dots) and the synthetic NLTE spectrum $T_{\text{eff}} = 14000\text{K}$, $\log g = 3.5$ (full line). Note the presence of telluric lines and bands near 6280\AA , $H\alpha$, 6870\AA , 7250\AA , and 7590\AA .

observed and model spectrum in the wings of Balmer lines (with the exception of $H\alpha$), while the Balmer line cores are affected by the emission. Quite satisfactory agreement was also achieved for the He I lines and for the Mg II 4481 Å line. Apart from $H\alpha$ wings, which are subject to high variability, the ratio between Mg II 4481 Å and He I 4471 Å is one of the best classification criteria for spectral types B7 – B8 (Steele et al. 1999). However, the synthetic Si II 6347 and 6371 Å lines are deeper than the observed ones which probably indicates that they are filled by a weak emission. A pronounced difference is seen for the infrared O I 7772, 7774, 7775 triplet, which is observed as a double-peak emission.

The Fe II lines studied by Hanuschik (1987) – namely the triplet 4924 Å, 5018 Å, 5169 Å, and somewhat weaker 4549 Å, 4584 Å, and 5316 Å lines – are also observed to have emission. On the other hand, there is no observable Fe II 6384 Å line in the spectra of κ Dra, similarly as for α Col from Hanuschik’s sample.

A casual inspection of the observed spectrum could lead to a conclusion that Fe II 4924 Å line has a P Cygni profile. Note, however, that this feature is in fact a blend of He I 4922 Å absorption and Fe II 4924 Å double peak emission. Similarly, the observed asymmetry of the emission peaks of Fe II 5018 Å line is also caused by blending with an absorption He I line at 5016 Å.

To see if there are any secular changes in the seemingly photospheric parts of the observed spectral lines we also compared the theoretical spectrum with the most recent spectrum of κ Dra corresponding to another phase of long-term changes. It turned out that the only changes are seen in the cores of the emission lines, especially of lower Balmer lines, and Fe II lines. The fit to the outer wings of higher lines of the Balmer series remains unchanged. This seems to indicate that any parts of the emission-line envelope are not contributing significantly to the observed continuum radiation or that their contribution was the same on both occasions.

4. Measurements

To investigate long-term variations of κ Dra, we focused on $H\alpha$, $H\beta$, $H\gamma$, $H\delta$, Si II 6347 Å, Si II 6371 Å, He I 6678 Å, and Fe II 6456 Å lines. We measured equivalent width W , peak intensities of the double emission lines, and the central intensity of the absorption reversals relative to the adjacent continuum (I_V , I_R and I_c , respectively) and also the peak separation between violet and red peaks ($\Delta\nu_p$). Note that W is taken with a negative sign for the emission line profile.

Both W and all intensities were measured in the original spectrum, i.e. without any subtraction of a synthetic spectrum (as it is sometimes done in similar studies) since this would imply an implicit assumption of an optically thin envelope. This need not be the case, especially in the cores of Balmer lines.

Only W and I_c were measured, of course, for the absorption lines of He and Si. All measurements are collected together with heliocentric Julian dates of mid-exposures (HJDs) in Tables 2, 3, and 4.

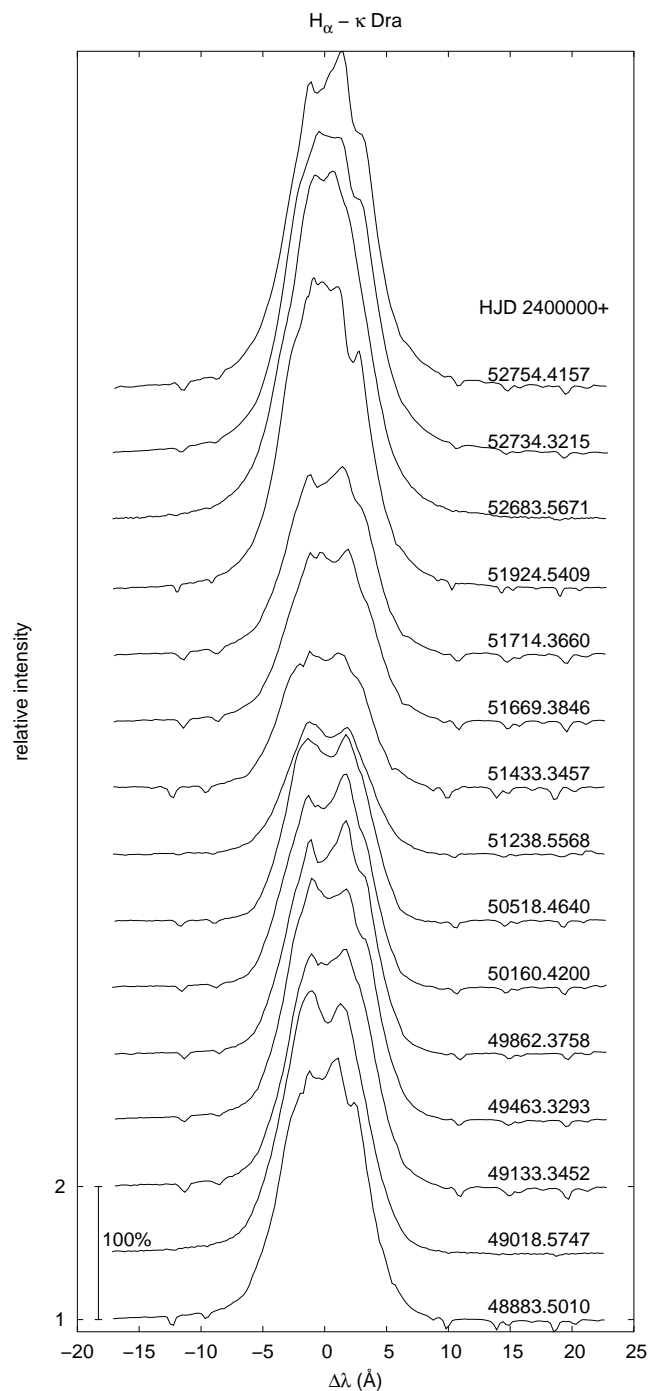


Fig. 3. Evolution of the $H\alpha$ intensity profile observed in κ Dra over the last 11 years. All spectra are normalized to the local continuum.

4.1. Balmer lines

4.1.1. Equivalent width (W)

$H\alpha$ line has always been observed as a double-peaked emission with a variable shape and strength (see Fig. 3). Fig. 4d shows the time variations of the $H\alpha$ equivalent width W during the past 30 years. Data prior to HJD 2448802.43819 were taken from Alvarez et al. (1990), Juza et al. (1994), and Moujtahid et al. (2000). Numerical values of W , shown only in a graphical form in Fig. 1 of Moujtahid et al. (2000) paper were kindly pro-

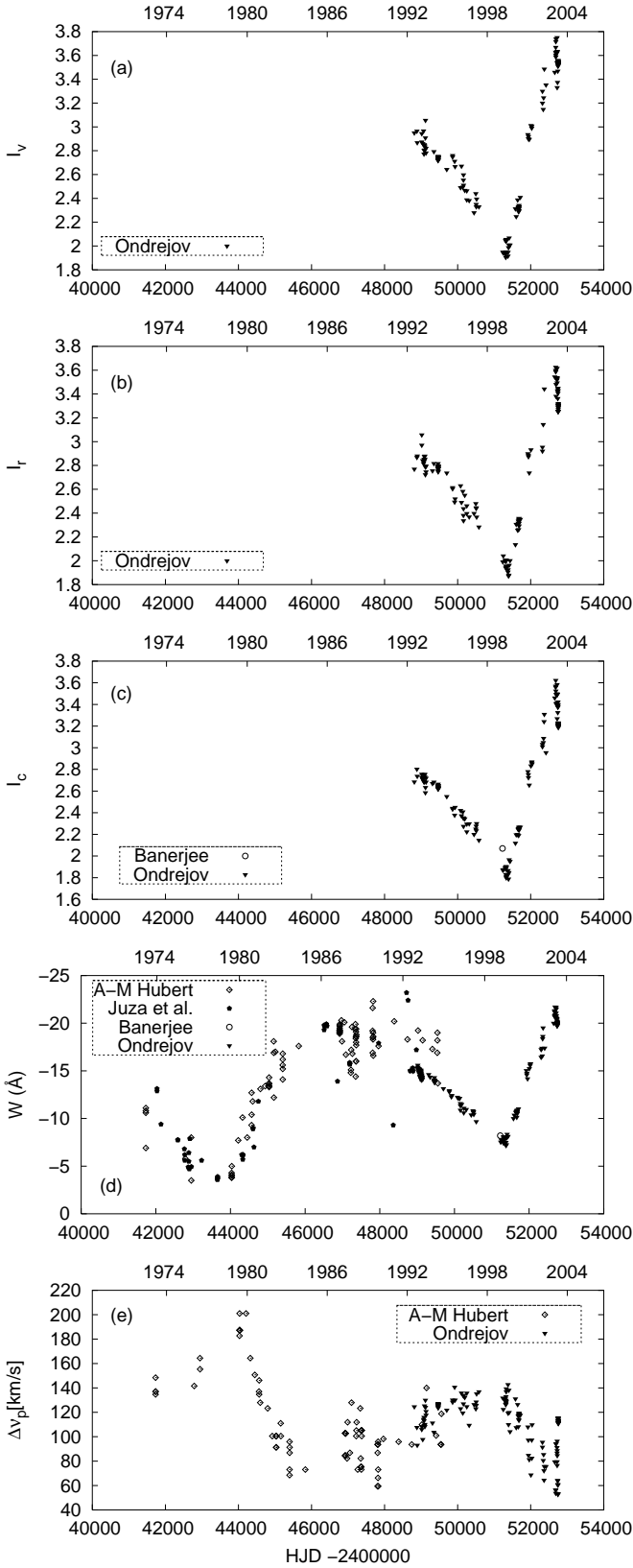


Fig. 4. Correlation between long-term variations of the H α emission line. (a) and (b): The relative intensity of the violet (I_V) and red (I_R) peaks, (c): relative central intensity of the line (I_c), (d): equivalent width of the H α line, (e): peak-separation $\Delta\nu_p$ (H α).

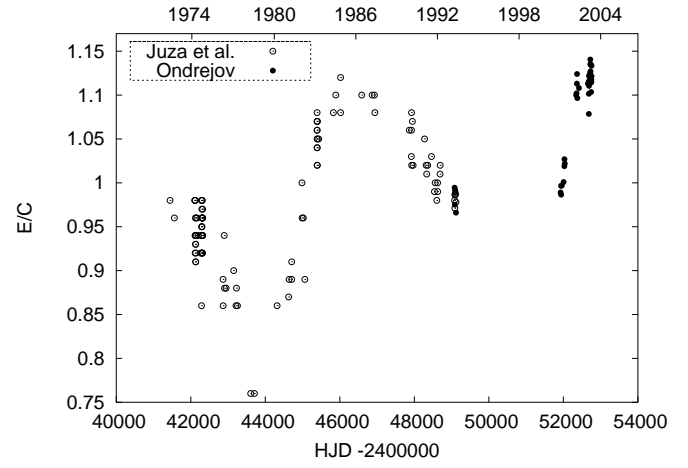


Fig. 5. Long-term variations of the E/C H β emission strength based on both, data from Juza et al. and new observations.

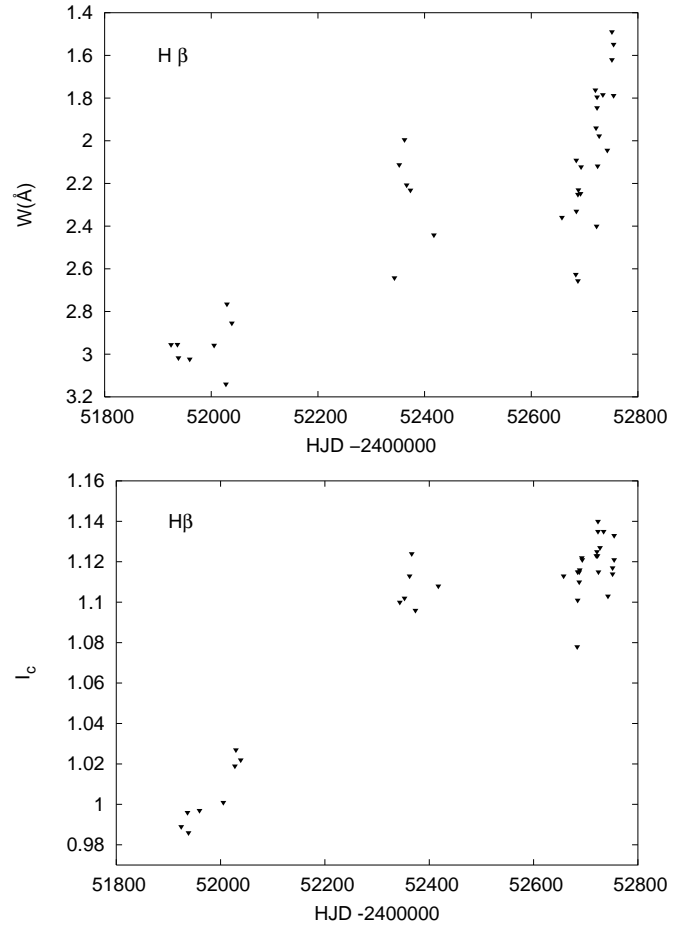


Fig. 6. Variations of H β equivalent width (upper panel) and intensity (lower panel).

vided to us by Dr. A.-M. Hubert. One measurement was taken from Banerjee et al. (2000). We recall again that the more negative values of the equivalent width the stronger the emission line.

The observations published earlier locate one minimum of the emission strength (the arithmetic maximum of W) into the

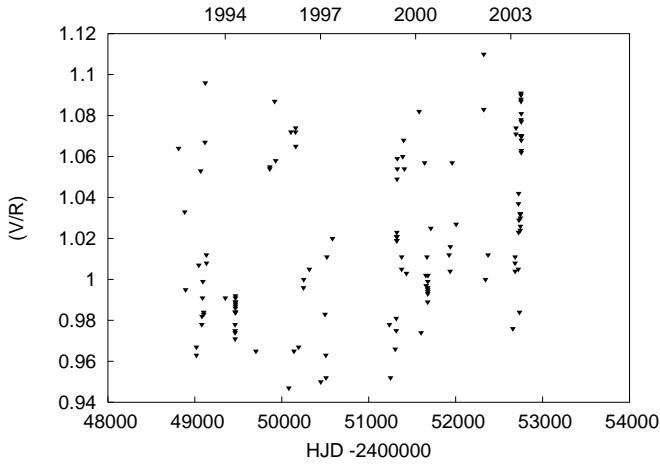


Fig. 7. A time plot of the V/R changes of $H\alpha$ emission line during the last 11 years. No long-term variations are observed.

interval between HJD 2443200 and 2443800, when $W_{H\alpha} \sim -3\text{\AA}$. The other, recent minimum is sharply defined by our data at HJD 2451380, when $W_{H\alpha}$ reached the value of -7.17\AA . With some scatter, the available data locate the time of the maximum emission around HJD 2447000 with a value of $W_{H\alpha}$ between -20\AA and -21\AA . The most recent data again indicate values near $W_{H\alpha} = -21\text{\AA}$ or lower.

Available equivalent widths of a $H\beta$ lines basically confirm the trend defined by $H\alpha$, though with an increased scatter. This is illustrated by the upper panel of a Fig. 6.

4.1.2. Central (I_c) and peak (E/C) line intensities

The central intensity I_c of the emission line we define as the intensity of the central part of the line relative to the continuum level. For the particular case of our star (α Dra) we measure it at the position of the central absorption. On the other hand, we can express the peak intensity by the ratio E/C , which is the mean intensity of both red and violet peaks, i.e. $(I_V + I_R)/2$. We measured the central intensities I_c for each line. For comparison with the data of Juza et al. (1994) we measured the intensity of $H\beta$ in terms of $(I_V + I_R)/2$ as well. Our measurements of the central intensity of $H\alpha$ were complemented by one observation published by Banerjee et al. (2000). The central intensity I_c shows parallel behavior with red (I_R) and violet (I_V) peak intensities, and also with $W_{H\alpha}$, as illustrated by the first four panels of Fig. 4.

Fig. 5 represents the intensity variation of $H\beta$ emission over the last 30 years. Data prior to HJD 2451924.5409 have been adapted from Juza et al. (1994). One can see a continuing cyclic variation over which a secular increase in the emission strength seems to be overlapped.

The central intensities of $H\gamma$ and $H\delta$ lines have been slowly increasing with time from 0.62 to 0.66, and from 0.53 to 0.56, respectively, over the period covered by our new data, showing again changes parallel to those seen in $H\alpha$.

Parallel changes of the intensity of the emission peaks I_V and I_R have been found for $H\alpha$. Note, however, that – in con-

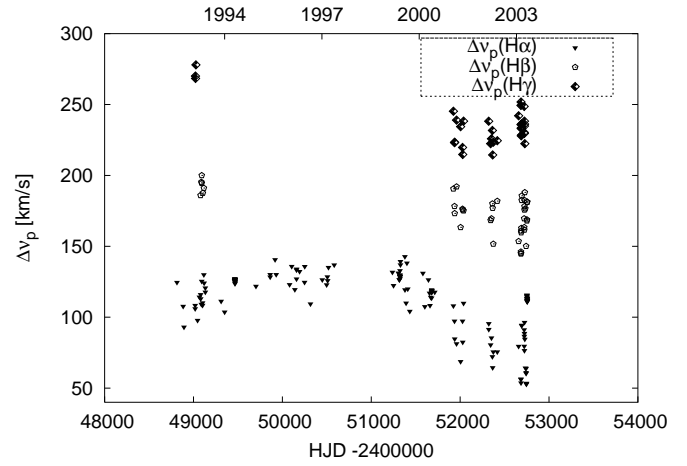


Fig. 8. Comparison of the peak separation of $H\alpha$, $H\beta$, and $H\gamma$ lines.

trast to many other Be stars – there is no clear evidence of parallel long-term V/R variations as Fig. 7 shows.

As shown already by Juza et al. (1991), this ratio exhibits phase-locked variations with phase of the 61^d55 binary orbit. We postpone investigation of orbital changes of α Dra into a follow-up study.

4.1.3. Peak separation ($\Delta\nu_p$)

Usually the double-peak structure is one of the characteristic features of the emission lines in Be stars. Peak-separations ($\Delta\nu_p$) were measured for Balmer lines whenever they were available in our α Dra spectra, the most prominent ones were in $H\alpha$, $H\beta$, and $H\gamma$ lines.

The $\Delta\nu_p$ of $H\alpha$ underwent very clear long-term variations over the interval covered by our data. After HJD 48802.43819 (in 1992) it started a gradual increase until it reached a maximum of 142 km s^{-1} at HJD 51378.5441 (in 1999). This was followed by a steep decrease to its minimum value of 53 km s^{-1} on HJD 52684.5418 (in 2003). Note that Arsenijević et al (1994) reported the maximum value of the peak separation of 206 km s^{-1} (in the years 1961–1962 and 1985–1986) and the minimum of 69 km s^{-1} in 1980. Fig. 4e displays the long-term behaviour of $H\alpha$ peak separation based on the new and compiled data. The first part of the $\Delta\nu_p$ long-term behaviour is mainly based on data from Moujtahid et al. (2000), kindly provided to us by Dr. A.-M. Hubert. They go from early 70's to 1995.

We also measured the peak separation for $H\beta$ and $H\gamma$ lines in all spectrograms, where these lines were available. Fig. 8 illustrates the comparison between the peak separation values of $H\alpha$, $H\beta$ and $H\gamma$. The measurements of $\Delta\nu_p(H\gamma)$ have large uncertainties because of weakness of the emission. Note that the values of $\Delta\nu_p(H\beta)$ are significantly higher than those of $H\alpha$, and smaller than $\Delta\nu_p(H\gamma)$. In particular, $\Delta\nu_p(H\gamma)$ ranges from 220 to 250 km s^{-1} , $\Delta\nu_p(H\beta)$ from 144 to 190 km s^{-1} and $\Delta\nu_p(H\alpha)$ from 53 to 108 km s^{-1} for the time interval where data for all three lines overlap. We observe that at any time the relation

$$\Delta\nu_p(H\alpha) < \Delta\nu_p(H\beta) < \Delta\nu_p(H\gamma) \quad (1)$$

holds. This reflects different regions of the formation of individual Balmer emission lines. The opacity in lower members of Balmer series is larger. Consequently, the lines are optically thick in the radial direction to a relatively large distance. This distance decreases with the increasing principal quantum number of the upper transition level. Higher members of the series originate at regions closer to the stellar surface, having higher Keplerian velocity, and therefore larger $\Delta\nu_p$.

Averaging the ratios $\Delta\nu_p(\text{H}\gamma)/\Delta\nu_p(\text{H}\alpha)$, $\Delta\nu_p(\text{H}\gamma)/\Delta\nu_p(\text{H}\beta)$, and $\Delta\nu_p(\text{H}\beta)/\Delta\nu_p(\text{H}\alpha)$ over all common epochs we can conclude that

$$\frac{\Delta\nu_p(\text{H}\gamma)}{\Delta\nu_p(\text{H}\alpha)} = 1.37 \pm 0.15 \quad (2a)$$

$$\frac{\Delta\nu_p(\text{H}\gamma)}{\Delta\nu_p(\text{H}\beta)} = 2.98 \pm 0.76 \quad (2b)$$

$$\frac{\Delta\nu_p(\text{H}\beta)}{\Delta\nu_p(\text{H}\alpha)} = 2.16 \pm 0.32 \quad (2c)$$

Within the errors, these ratios are close to the mean values estimated by Hanuschik et al. (1988) and Dachs et al. (1992):

$$\frac{\Delta\nu_p(\text{H}\beta)}{\Delta\nu_p(\text{H}\alpha)} \approx 1.8 \pm 0.5 \quad (3a)$$

$$\Delta\nu_p(\text{H}\gamma) \approx 1.2\Delta\nu_p(\text{H}\beta) \approx 2.2\Delta\nu_p(\text{H}\alpha), \quad (3b)$$

for Be stars having symmetric double-peak profiles.

4.2. Other lines

The lines of Si II 6347 Å, Si II 6371 Å, Fe II 6456 Å, and He I 6678 Å are all relatively weak in comparison to the Balmer lines but in most cases their measurements were reliable enough. The silicon lines Si II 6347 Å and Si II 6371 Å, and the helium line He I 6678 Å have been in absorption, while the Fe II 6456 Å line has appeared as a double-peaked emission profile during all 11 years of observations. The line profiles of He I 6678 Å and Fe II 6456 Å are shown in Figs. 9 and 10, respectively. Note that at certain times it was quite difficult to measure these weak lines because of a heavy blending with neighbouring telluric lines.

He I 6678 Å is the strongest absorption line besides H α in the red part of the spectrum. It appears as a shallow absorption line with an intensity 0.04 relative to the continuum level (see Fig. 9). Its equivalent width varies from 0.12 Å to 0.22 Å from the early 1992 to 1999 and then decreases, with large fluctuations, to 0.1 Å (see lower panel of Fig. 11). In spite of the scatter, one can see that He I 6678 Å equivalent width follows the same trend as the emission lines of H α and Fe II 6456 Å.

Both Si II 6347 Å and Si II 6371 Å lines exhibit variations in their equivalent width from 0.04 Å to 0.1 Å at most, as shown in the upper and middle panels of Fig. 11. In spite of a considerable scatter, one can recognize a monotonous decrease of their equivalent width with time.

Line profile of Fe II 6456 Å appears permanently as a double emission (see Fig. 10). Its central intensity I_c is gradually

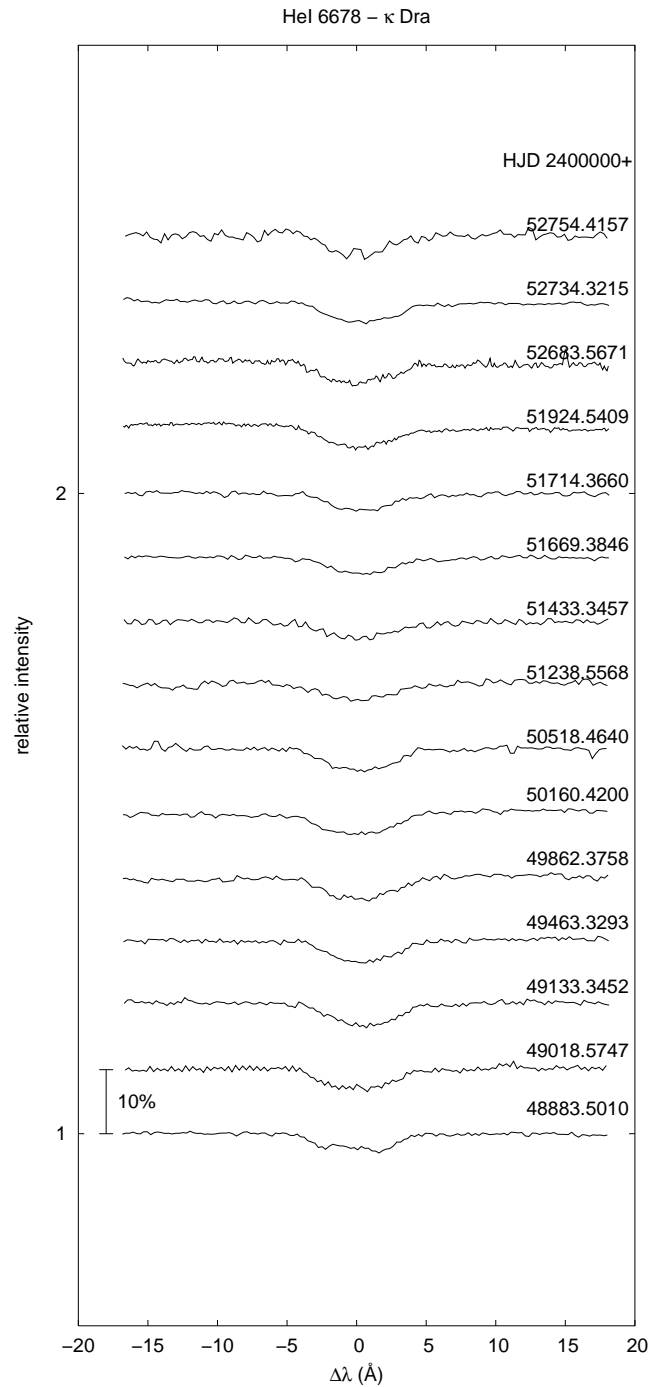


Fig. 9. Evolution of the He I 6678 Å intensity profile observed in κ Dra over the last 11 years. All spectra are normalized to the local continuum.

varying between 0.98 and 1.06 and back, in parallel to the variations of the Balmer lines; The equivalent width of this line increases (with fluctuations) from the value of -0.17 Å in 1992 to -0.05 Å in 1999 (see Fig. 12). Between 2000 and 2003 the emission strengthens rapidly so that the equivalent width arithmetically decreases, reaching its lowest value of -0.5 Å during the most recent observations. The epochs when the Fe II 6456 Å line is either very faint or completely missing, correlates well with phases of weakest H α emission.

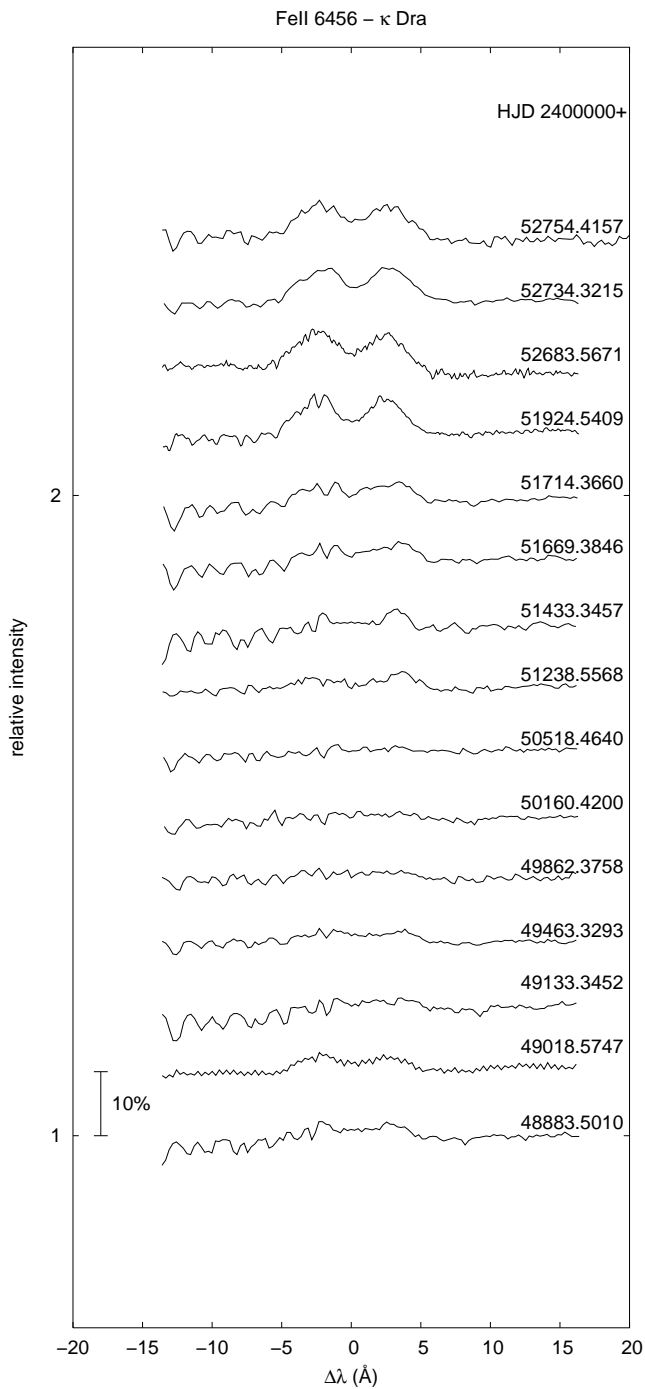


Fig. 10. Evolution of the Fe II 6456 Å intensity profile observed in κ Dra over the last 11 years. All spectra are normalized to the local continuum.

Central intensities of He I 6678 Å line, and of both Si II 6347 Å and 6371 Å lines are subject to a large scatter and are not displayed.

4.3. Photometry

Long-term variations of the V magnitude and of both $B - V$ and $U - B$ indices are shown in the Fig. 13 in the form of 1-

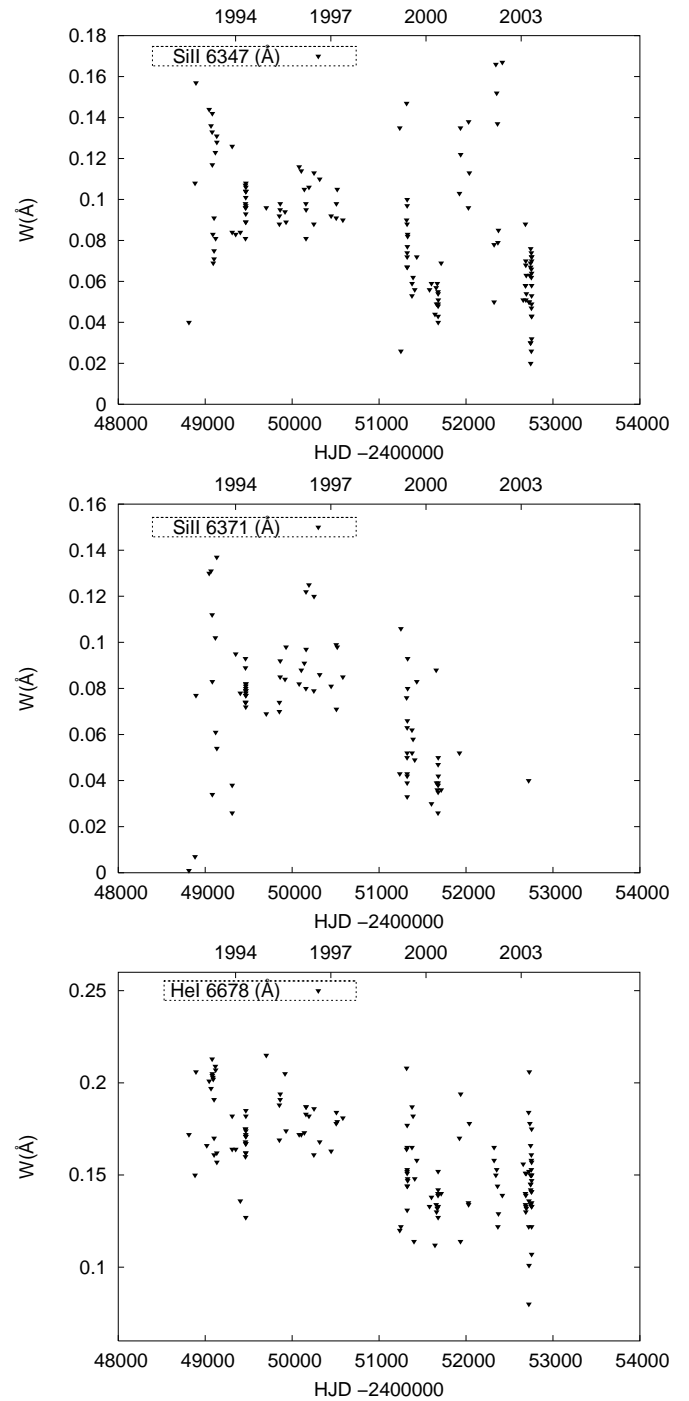


Fig. 11. Long-term variations of the equivalent width of Si II 6347 Å line (upper panel), Si II 6371 Å line (middle panel), and He I 6678 Å (lower panel).

d normals. One can see that the brightness in the V passband clearly correlates with the long-term spectral changes.

Besides, it is clear that occasional smaller brightenings or fadings occur on a much shorter time scale than the long-term ones. While it is conceivable that a single case of such a behavior could be blamed for larger observational errors, we want to point out that, e.g., the sudden brightening observed at Hvar on HJD 2451377.4, is undoubtedly a real phenomenon. This normal point is based on three observations giving a small rms

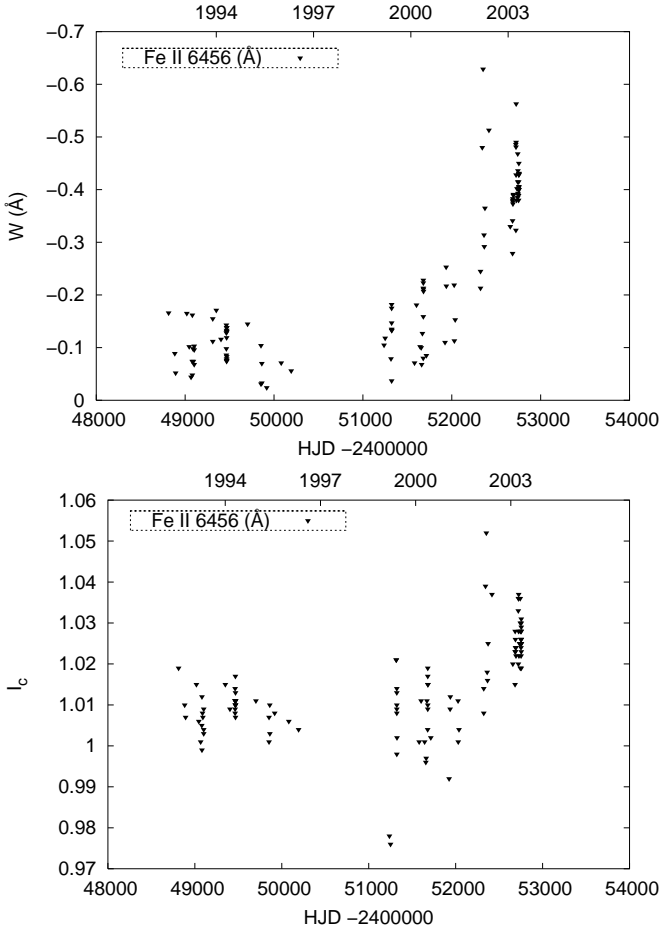


Fig. 12. Long-term variations of Fe II 6456 Å line equivalent width (upper panel) and intensity (lower panel).

error of the mean, obtained on a good night with measured extinction and normal values observed for the check star. Such brightenings were also observed for some other long-term Be variables, e.g. ω CMa (HD 56139) – see Fig. 8 in Harmanec (1998b).

5. Basic physical properties of α Dra

Most of published spectral classifications of α Dra agree on the spectral class B5IIIe–B6IIIe – cf., e.g., Slettebak (1982), Hoffleit & Jaschek (1982). The effective temperature derived here from the line-profile modelling corresponds to spectral class B6.

One may carry out several consistency checks. First, one can use the accurate Hipparcos parallax of α Dra (6.55 ± 0.55) mas (Perryman et al. 1997) and a properly chosen V magnitude to an estimate of the stellar radius. As already mentioned, the star has never been observed without emission. However, in the period with only a very weak emission around HJD 2443700 the V magnitude of the object attained a minimum brightness of about $3^m.97$. Interstellar reddening of α Dra was derived by Beeckmans & Hubert-Delplace (1980). Three different methods consistently led to $E(B - V) = 0^m.04$. Using the unreddened magnitude $V_0 = 3^m.93$, bolometric correction from Code et al. (1976), and the Hipparcos parallax, one

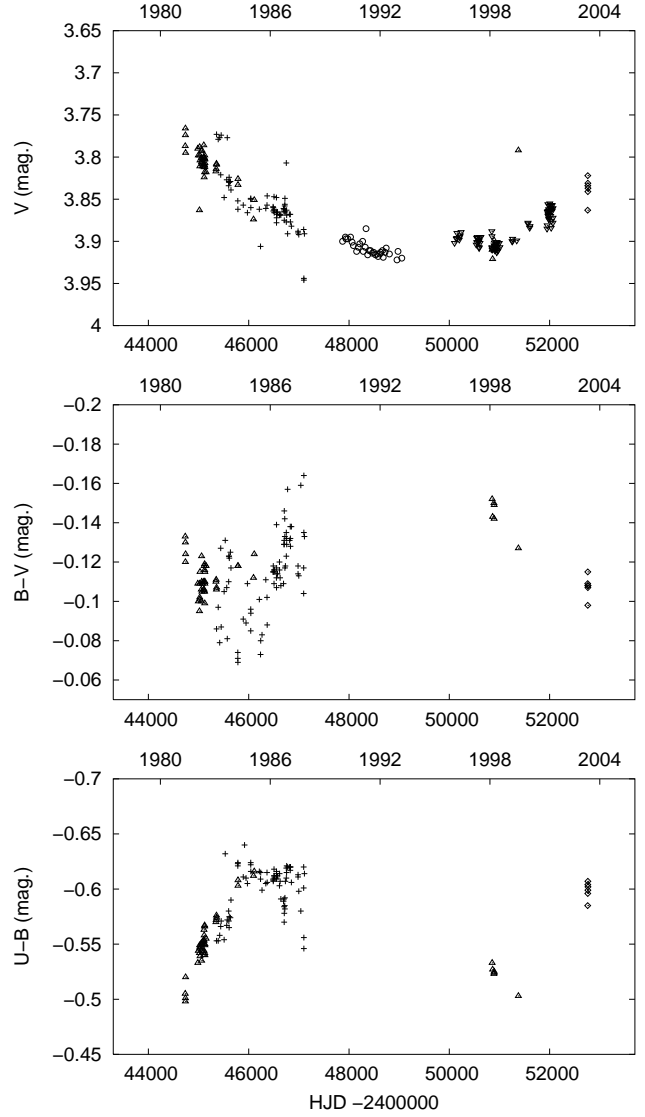


Fig. 13. Photometry of α Dra from Hvar (Δ), Skalnaté Pleso (+), and Tubitak (\diamond) observatories, from the Hipparcos satellite (\circ) and from Crossall et al. (2001 – ∇).

obtains

$$R = 6.4 \pm 0.5 R_{\odot}. \quad (4)$$

The spectroscopic mass which follows from the comparison with the model atmosphere and $\log g = 3.5$ is then

$$M = 4.8 \pm 0.8 M_{\odot}. \quad (5)$$

Errors in the Eqs. (4) and (5) reflect the error of the parallax.

In Fig. 14 we compare the stellar radius derived above with Schaller's et al. (1992) evolutionary tracks for 5 and 7 M_{\odot} models stars. One can see that the position of α Dra corresponds to a giant star, evolved close to the terminal-age main sequence (TAMS) and having a mass slightly over 5 M_{\odot} . For solar composition, the corresponding evolutionary age is something like $8 \cdot 10^7$ years. The bolometric magnitude of the star is $-3^m.1$.

It is encouraging to see that in spite of all uncertainties, we arrived at consistent estimates of the mass of the Be star by two

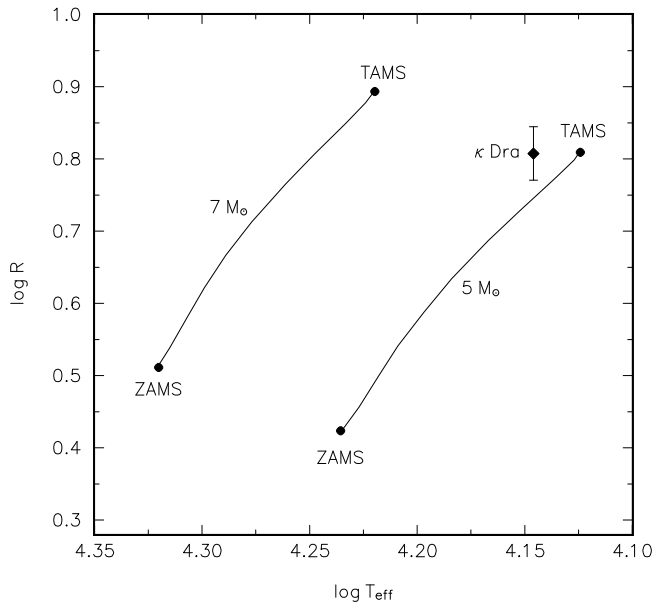


Fig. 14. The position of κ Dra in the $\log R$ vs. $\log T_{\text{eff}}$ diagram. Schaller's et al. (1992) evolutionary models for $5 M_{\odot}$ and $7 M_{\odot}$ stars are shown by solid lines.

independent methods. This is very important since just the lack of direct determinations of stellar masses of Be stars is one of the sources of uncertainty in considerations about how close the rotation of Be stars is to break up velocity at the equator.

6. Character of long-term variations

During the past century, κ Dra has shown very pronounced spectral variability. The strength of $H\beta$ emission was found to vary on a scale of about two decades. While such variations of Be stars were usually found to be cyclic with variable length of individual cycles, in the case of κ Dra several authors argued in favour of a real periodicity. Periods of 30 and 23 years for the variation of E/C of $H\beta$ have been suggested by Struve (1925) and Jessup (1932), respectively. McLaughlin (1937) noted that in 1936 the emission at $H\beta$ and $H\alpha$ had almost disappeared. Alvarez et al. (1990) reported that the $H\alpha$ line equivalent width varies between 5 \AA and 25 \AA . As their Figure 1 shows, they also found a clear correlation between continuum polarization and $W_{H\alpha}$. This correlation was later confirmed by a large series of observations published by Arsenijević et al. (1994).

Juza et al. (1994) summarized the history of the investigation of κ Dra up to 1993. They collected and homogenized all published records of spectral, light, and polarimetric variations and combined them with their own series of spectral and UBV observations. They found secular changes in V , B , $B-V$, and $U-B$, correlated with changes of the strength of Balmer emission lines. Notably enough, the U magnitude only exhibited small, possibly cyclic variations but no secular changes.

Juza et al. (1994) analyzed all homogenized records of the E/C strength of the $H\beta$ emission for periodicity and concluded that it varies with a period of 8406 ± 23 days

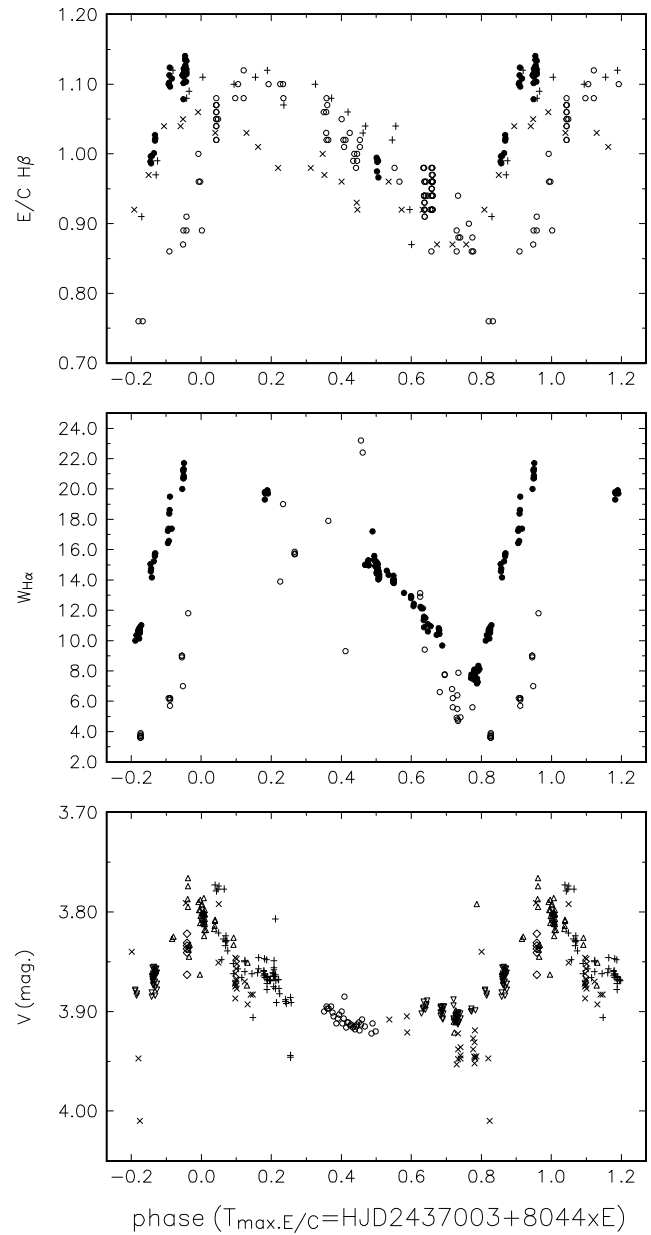


Fig. 15. A phase plot of the $H\beta$ E/C emission strength, $W_{H\alpha}$ and V magnitude of κ Dra vs. phase of the 8040-d period. In the first panel, crosses denote the estimates compiled by Jessup (JD 2412450-26680), pluses those by Curtiss (JD 2419546-25751), open circles refer to measurements from photographic spectra published by Juza et al. (JD 2441443-46587) and filled circles are our measurements in electronic spectra (JD 49079-52754). In the central panel, open and filled circles refer to equivalent width measured in photographic and electronic spectra, respectively. For V photometry, the same notation is used as in Fig. 13.

(23.01 years). From the records of the equivalent width $W_{H\alpha}$ they found the same period of 8400 ± 340 days.

6.1. Determination of a long term period

Having new longer series of observations at our disposal, we repeated the period analysis of Juza et al. (1994) but with the following modifications.

The principal data set, covering the longest time interval from JD 2412450 to JD 2452754 is represented by various records of the $H\beta$ emission strength, E/C . A proper period analysis of these observations is a bit tricky. As we already mentioned, we prefer to analyze directly observable quantities. For E/C we adopt the observed peak intensity of the emission, measured in units of local continuum, i.e. $(I_V + I_R)/2$, similarly as Juza et al. (1994) did. Older observations, based on visual estimates, were homogenized and brought onto this scale already by Juza et al. but come from two principal sources which we treat separately. The third data set is represented by measurements from photographic spectra and the last and the most accurate one comes from electronic spectra. It is quite probable that the zero points of the E/C scale for the above mentioned four data subsets differ. We allowed for it and the period analysis then showed that all data can be reconciled quite well with a period of (8044 ± 157) days, the epoch of the maximum strength being (HJD 2437003 ± 55)d, i.e. 22.0 years, which is for about one year shorter than the previous estimate.

Then we kept this period fixed and analyzed $W_{H\alpha}$, this time allowing for a zero-point difference only between photographic and electronic spectra. This data set spans a time interval JD 2434437 – 2452693. Finally, we also folded all V magnitude observations, spanning JD 2435400 – 2452827, with the same period. The phase plot for all three observables is shown in Fig. 15.

The E/C data now span full 5 cycles. It is immediately seen that they can be folded with the 8044-d period to the point that the maxima and minima are approximately presented but one can also see the individuality of various cycles. For instance, the latest cycle is distinctly narrower than the previous one. Note that the period of 8400 days determined by Juza et al. (1994) predicts the the time of minimum $W_{H\alpha}$ for the year 2002 while the actual time of minimum came in 1999, i.e., three years earlier. Moreover, the time span between two latest events of a steep rise of the $H\alpha$ emission (cf. Fig. 4d) is ~ 6900 days. This puts serious doubts on a strict periodicity.

On the other hand, the mutual phase agreement of three *independent* data sets in Fig. 15 looks quite impressive and there are numerous examples among Be stars which display cyclic phenomena with very variable individual cycle length and shape. Therefore, the possibility of whether the whole phenomenon is not controlled by some regular clock deserves further study.

6.2. Discussion of long-term variations

The question is how to interpret these spectacular long-term changes. Already Juza et al. (1994) pointed out that the character of long-term variations of α Dra is typical for a positive correlation between brightness and emission strength as defined by Harmanec (1983). They also noted that the rise of the emission strength is much steeper than its decline. From this fact, they

concluded that there must be some, as yet unknown, physical mechanism which supplies fresh material into the circumstellar envelope every 23 years.

A phase lag between the maximum brightness and maximum emission strength found by Juza et al. (1994) has been confirmed. This again agrees with the idea of two types of a correlation between the brightness and emission strength (cf. Harmanec 2000). For an inverse correlation (opposite to that observed for α Dra, this was discussed semi-quantitatively by Koubský et al. (1997): When a new envelope is formed, it first adopts the form of a relatively small region which is optically thick in the optical continuum (called “pseudophotosphere” by Harmanec 1983, 2000). If the star is observed more pole-on than equator-on (and this is the case of α Dra), the inner parts of the disk effectively increase the apparent radius of the star. This leads to an increasing brightness of the object. As the envelope grows in extent and rarefies, it becomes optically thin in continuum and one observes increasingly strong Balmer emission and the brightness begins to decrease again.

A very similar interpretation of the activity cycle was put forward also by Hirata (1995) who, however, modelled the optically thick parts of the envelope explicitly as gravitationally darkened stellar photospheres rotating close to the break-up speed. We note that his approach is only legitimate if the envelope is formed by a gradual outflow of the material from the stellar photosphere.

In principle, one can envision the following *qualitative* interpretations of the long-term changes observed:

- One possibility is that the long-term variations of α Dra are manifestations of the still mysterious Be phenomenon. Even so, the interesting aspect is that the re-appearance of the emission is rather regular and that the envelope never disappears completely as it is the case for many other Be stars. If this explanation is accepted, α Dra is indeed a good example of the object with a positive correlation between brightness and emission strength.
- Another possibility is to assume that the re-appearance of the emission is a periodic phenomenon. The fact that different cycles do not repeat perfectly need not be an ultimate argument against such a possibility since there are many examples of periodic phenomena with cycle-to-cycle variations, like X-ray flares in Be+X binaries or even light curves of Be stars in binary systems. To the best of our knowledge, there are no speckle-interferometric observations of α Dra and the idea that the formation of a new envelope occurs during periastron passage of a putative companion to α Dra moving in an eccentric orbit is a reasonable working hypothesis to be tested by future observations.

7. Summary

This study is essentially devoted to the investigation of the long-term variations and of the physical properties of the Be star α Dra. We have presented and analysed new set of spectroscopic observations obtained between 1992 – 2003. We also used the published records of the star.

Spectrograms obtained during last three years of observations cover a wide range of the wavelengths (3450 – 8860 Å). These wide range spectra were used for a detailed line identification in the visible and near infrared range and for a comparison with synthetic spectra calculated from NLTE model atmospheres (Section 3.1). The best fit was found for a model with $T_{\text{eff}}=14\,000\text{K}$, $\log g = 3.5$ and $v \sin i = 170 \text{ km s}^{-1}$. However, it is only an approximate estimate, since we considered an oversimplified picture of the atmosphere as a plane-parallel and static one. From the available photometric records, parallax, and from the model atmosphere we obtained the stellar radius $R_* = 6.4R_{\odot}$, and mass $M_* = 4.8M_{\odot}$.

An analysis of time variations of the line strength (equivalent width) and intensity of H α and H β over the last thirty years show that α Dra undergoes cyclic long-term variations with an average cycle of 22 years. These cyclic changes are most probably caused by a steep rise and a gradual decrease of the dimensions of a rapidly rotating circumstellar disk. This picture is supported by the fact that for stronger Balmer line emission, formed in more distant (and not so fastly rotating) regions of the disk, the peak separation gets also smaller. This is observed both for individual Balmer emission lines at the same spectrograms and for temporal evolution of each of the Balmer lines.

There remain unsolved problems, however. First, the true physical origin of a 22 year variation cycle is unknown. It is probably caused by disk oscillations, but that is all we are able to say now. Second, the fact that the helium lines are in absorption while hydrogen and iron lines are in emission is also not explained. More detailed modelling of a hydrodynamics and radiative transfer in a disk will help to improve the basic physical parameters of this star.

Acknowledgements. Some of the *Reticon* spectra from the archive of the Ondřejov 2m-telescope (see Škoda 2000) have been secured by Drs. J. Horn, K. Juza, V. Šimon, and S. Štefl. The authors would like to thank the technical staff of the 2m-telescope (J. Havelka, J. Honsa, K. Kalaš, L. Řezba, L. Šarounová, M. Tlamicha, and F. Žďárský) for their help with the observations. Our thanks are also due to Dr. A.-M. Hubert who kindly gave their quantitative measurements of the H α profiles at our disposal and to Dr. Karen Bjorkman who kindly provided us with a copy of an unpublished poster paper. This research has made use of the NASA's Astrophysics Data System Abstract Service (Kurtz et al. 2000, Eichhorn et al. 2000, Accomazzi et al. 2000, Grant et al. 2000) and the CDS bibliographical service. Our work was supported by grants of Grant Agency of the Czech Republic 205/02/0445 and 205/03/0788. Astronomical Institute Ondřejov is supported by projects K2043105 and Z1003909. Astronomical Institute of the Charles University is supported via research plan J13/98: 113200004 of MŠMT.

References

- Accomazzi, A., Eichhorn, G., Kurtz, M. J., Grant, C. S., & Murray, S. S. 2000, *A&AS* 143, 85
- Alvarez, M., Hubert-Delplace, A.-M., Arsenijević, J., Ballereau, D., & Chauville, J. 1990, *Rev. Mex. Astron. Astrof.* 21, 398
- Arsenijević, J., Jankov, S., Krsljanin, S., et al. 1994, in *IAU Symp.* 162, Pulsation, Rotation and Mass Loss in Early-Type Stars, L. Balona, H. Henrichs & J. M. LeContel eds., Kluwer Academic Publ., Dordrecht, p. 234
- Ballereau, D., & Chauville, J. 1987, *A&AS* 70, 229
- Banerjee, D. P. K., Rawat, S. D., & Janardhan, P. 2000, *A&AS* 147, 229
- Beeckmans, F., Hubert-Delplace, A.-M. 1980, *A&A* 86, 72
- Campbell, W. W. 1895, *ApJ* 2, 177
- Chalonge D., Divan L. 1952, *Ann. Astrophys.* 15, 201
- Chauville, J., Zorec, J., Ballereau, D., et al. 2001, *A&A* 378, 861
- Code, A. D., Davis, J., Bless, R. C., Hanbury Brown, R. 1976, *ApJ* 203, 417
- Croxall, K. V., Morisson, N. D., Bjorkman, K. S., 2001, poster #133.07 at the 199th AAS meeting
- Dachs, J., Hummel, W., & Hanuschik, R. W. 1992, *A&AS* 95, 437
- Eichhorn, G., Kurtz, M. J., Accomazzi, A., Grant, C. S., & Murray, S. S. 2000, *A&AS* 143, 61
- Grant, C. S., Accomazzi, A., Eichhorn, G., Kurtz, M. J., & Murray, S. S. 2000, *A&AS* 143, 111
- Gray, D. F., 1976, *Observation and Analysis of Stellar Photospheres*, John Wiley & Sons, New York
- Guo, Y., Huang, L., Hao, J., Cao, Z., & Guo, X. 1995, *A&AS* 112, 201
- Hao, J. 1994, *BeSN* 28, 9
- Hanuschik, R. 1987, *A&A* 173, 299
- Hanuschik, R. W., Kozok, J. R., & Kaiser, D. 1988, *A&A* 189, 147
- Harmanec, P. 1983, *Hvar Obs. Bull.* 7, 55
- Harmanec, P. 1988, *Bull. Astron. Inst. Czechosl.* 39, 329
- Harmanec, P. 1998a, *A&A* 334, 558
- Harmanec, P. 1998b, *A&A* 335, 173
- Harmanec, P. 2000, in *The Be Phenomenon in Early Type Stars*, IAU Coll. 175, M. A. Smith, H. F. Henrichs, & J. Fabregat eds., ASP Conf. Ser. Vol. 214, p. 13
- Harmanec, P. 2003, in *Workshop On "New Directions For Close Binary Studies: The Royal Road To The Stars"*, Canakkale Onsekiz Mart University Publication 3, 221
- Harmanec, P., Horn, J. 1998, *Journal of Astronomical Data* 4, CD-ROM file 5
- Harmanec, P., Horn, J., Juza, K. 1994, *A&AS*, 104, 121
- Harmanec, P., Bisikalo, D. V., Boyarchuk, A. A., & Kuznetsov, O. A. 2002, *A&A* 396, 937
- Hirata, R. 1995, *PASJ* 47, 195
- Hirata, R., & Kogure, T. 1984, *Bull. Astron. Soc. India* 12, 109
- Hill, G. M., Walker, G. A. H., & Yang, S. 1991, *A&A* 246, 146
- Hoffleit, D., & Jaschek, C. 1982, *The Bright Star Catalogue*, 4th Edition, Yale Univ. Obs., New Haven, USA
- Horn, J., Hubert, A. M., Hubert, H., Koubský, P., & Bailloux, N. 1992, *A&A* 259, L5
- Horn, J., Kubát, J., Harmanec, P., et al. 1996, *A&A* 309, 521
- Huang, S. S. 1972, *ApJ* 171, 549
- Hubert, H. 1971, *A&A* 11, 100
- Hutchings, J. B. 1971, *MNRAS* 152, 109
- Jessup, M. K. 1932, *ApJ* 76, 75
- Johnson, H. L., Mitchell, R. I., Iriarte, B., Wiśniewski, W. Z. 1966, *Com. Lunar Planet. Obs.* 4, 99
- Juza, K., Harmanec, P., Hill, G. M., et al. 1991, *Bull. Astron. Inst. Czechosl.* 42, 39.
- Juza, K., Harmanec, P., Božić, H., et al. 1994, *A&AS* 107, 403.
- Koubský, P., Harmanec, P., Kubát, J., et al. 1997, *A&A* 328, 551
- Koubský, P., Harmanec, P., Hubert, A.-M., et al. 2000, *A&A* 356, 913
- Kubát, J. 1999, *NewA* 4, 157
- Kubát, J. 2003, in *Modelling of Stellar Atmospheres*, IAU Symp. 210, N. E. Piskunov, W. W. Weiss, & D. F. Gray eds., ASP Conf. Ser., in press
- Kurtz, M. J., Eichhorn, G., Accomazzi, A., et al. 2000, *A&AS* 143, 41
- McLaughlin, D. B. 1937 *ApJ* 85, 181

- Moujtahid, A., Hubert, A. M., Zorec, J., et al. 2000, in *The Be Phenomenon in Early Type Stars*, IAU Coll. 175, M. A. Smith, H. F. Henrichs, & J. Fabregat eds., ASP Conf. Ser. Vol. 214, p. 514
- Perryman, M. A. C., Høg, E., Kovalevsky, J., Lindegren, L., & Turon, C. 1997, *ESA SP-1200: The Hipparcos and Tycho Catalogues*
- Popper, D. M. 1980, *ARA&A* 18, 115
- Prinja, R. K. 1989, *MNRAS* 241, 721
- Schaller, G., Schaerer, D., Meynet, G., & Maeder, A. 1992, *A&AS*, 96, 269
- Škoda, P. 1996, in *Astronomical Data Analysis Software and Systems V*, G. H. Jacoby & J. Barnes eds., ASP Conf. Ser. Vol. 101, p. 187.
- Škoda, P. 2000, in *Astronomical Data Analysis Software and Systems IX*, N. Manset, C. Veillet, & D. Crabtree eds., ASP Conf. Ser. Vol. 216, 153
- Škoda, P., & Šlechta, M. 2002, *Publ. Astron. Inst. Czech* 99, 1
- Steele, I. A., Negueruela, I., and Clark, J. S., 1999, *A&AS*, 137, 147.
- Slettebak, A., 1982, *ApJS* 50, 55
- Stahl, O., Kaufer, A., Wolf, B., et al. 1995, *The Journal of Astronomical Data* 3, 1 (on CD-ROM)
- Štefl, S., & Rivinius, T. 2000, in *The Be Phenomenon in Early Type Stars*, IAU Coll. 175, M. A. Smith, H. F. Henrichs, & J. Fabregat eds., ASP Conf. Ser. Vol. 214, p. 356
- Stoeckley, T. R., Buscombe, W. 1987, *MNRAS* 227, 801
- Struve, O. 1925, *Pop. Astron.* 33, 596

Online Material

In all tables, W is the equivalent width, I_c is the central line intensity, I_V and I_R are the violet and red emission peak intensities, respectively, $\Delta\nu_p$ is the velocity difference between red and violet peaks, and V/R is the violet-to-red peak ratio. The sign — means that the corresponding quantity was not measurable.

Table 2. Measured parameters of the H α emission line.

File	HJD –2400000	$W_{H\alpha}$ [Å]	I_c	I_V	I_R	$\Delta\nu_p$ [km s $^{-1}$]	V/R
R00311	48813.4315	–14.99	2.68	2.95	2.77	124.5	1.06
R00685	48883.5010	–15.27	2.80	2.96	2.86	107.6	1.03
R00743	48893.2294	–14.96	2.73	2.86	2.88	93.05	0.99
R00939	49018.5005	–15.59	2.75	2.94	3.05	108.3	0.96
R00940	49018.5747	–15.38	2.72	2.87	2.97	106.0	0.96
R01270	49045.4875	–14.92	2.70	2.86	2.84	97.70	1.00
R01303	49066.4515	–15.15	2.72	2.96	2.81	114.1	1.05
R01381	49079.5350	–14.46	2.68	2.77	2.83	115.9	0.97
R01448	49081.4524	–14.41	2.68	2.80	2.85	113.0	0.98
R01465	49088.3750	–14.96	2.75	2.85	2.87	109.1	0.99
R01515	49092.4614	–14.71	2.72	2.84	2.84	125.3	0.99
R01566	49102.3636	–14.78	2.72	2.80	2.85	110.1	0.98
R01568	49102.3818	–15.07	2.75	2.83	2.87	108.3	0.98
R01697	49116.4731	–14.03	2.58	2.90	2.72	129.9	1.06
R01740	49119.5657	–14.57	2.63	3.05	2.78	124.1	1.09
R01839	49133.3452	–14.12	2.68	2.78	2.74	120.7	1.01
R01849	49133.4032	–14.30	2.71	2.82	2.79	117.7	1.00
R03467	49310.6279	–14.61	2.67	—	2.75	111.3	—
R03601	49350.6331	–14.34	2.68	2.79	2.81	103.6	0.99
R04243	49463.3294	–14.28	2.66	2.73	2.81	125.9	0.97
R04249	49463.3564	–13.99	2.64	2.71	2.78	127.1	0.97
R04261	49463.4929	–14.04	2.65	2.72	2.79	125.9	0.97
R04274	49463.5259	–13.90	2.64	2.72	2.78	125.9	0.97
R04406	49466.3311	–13.98	2.62	2.74	2.79	126.5	0.98
R04407	49466.3459	–13.86	2.62	2.74	2.77	123.6	0.98
R04427	49466.3994	–13.88	2.62	2.74	2.77	126.5	0.98
R04433	49466.4142	–13.83	2.62	2.74	2.77	126.5	0.99
R04445	49466.5338	–13.95	2.62	2.75	2.79	127.1	0.98
R04446	49466.5492	–13.97	2.63	2.74	2.79	126.6	0.98
R04462	49466.6149	–13.96	2.62	2.75	2.79	126.5	0.98
R04469	49467.3034	–14.03	2.64	2.74	2.77	124.2	0.99
R04484	49467.3497	–13.98	2.65	2.74	2.77	125.3	0.99
R04496	49467.4651	–13.79	2.63	2.72	2.74	124.8	0.99
R04515	49467.5566	–13.82	2.63	2.73	2.75	125.4	0.99
R07348	49702.6550	–13.14	2.55	2.64	2.73	121.8	0.96
R08190	49862.3759	–12.80	2.43	2.74	2.60	128.3	1.05
R08191	49862.3842	–12.92	2.44	2.76	2.61	130.1	1.05
R08551	49918.3372	–12.28	2.37	2.71	2.49	140.6	1.09
R08739	49930.3387	–12.42	2.45	2.66	2.52	130.1	1.06
R09690	50080.6261	–12.23	2.42	2.49	2.63	123.0	0.95
R09862	50104.7034	–12.13	2.37	2.67	2.49	135.9	1.07
R10089	50140.5900	–12.12	2.41	2.49	2.58	119.5	0.96
R10245	50158.5779	–11.35	2.35	2.55	2.38	126.9	1.07
R10268	50159.4882	–10.87	2.27	2.51	2.33	133.4	1.07
R10285	50160.4201	–11.57	2.35	2.59	2.43	133.9	1.06
R10562	50193.4706	–11.49	2.34	2.46	2.55	132.2	0.96
R10972	50249.4667	–10.60	2.22	2.38	2.39	124.6	0.99
R10995	50251.3830	–11.08	2.29	2.46	2.46	135.8	1.00
R11509	50316.3418	–10.95	2.29	2.38	2.36	109.4	1.00
R12257	50448.6371	–10.38	2.20	2.28	2.39	126.4	0.95
R12528	50497.4534	–10.82	2.24	2.44	2.48	122.8	0.98
R12576	50506.5231	–10.71	2.27	2.35	2.44	128.5	0.96
R12619	50509.529	–10.66	2.23	2.33	2.44	125.7	0.95
R12743	50518.464	–10.44	2.30	2.39	2.36	135.2	1.01

Table 2. – continued

File	HJD –2400000	$W_{H\alpha}$ [Å]	I_c	I_V	I_R	$\Delta\nu_p$ [km s ⁻¹]	V/R
R13044	50583.4009	–9.676	2.14	2.33	2.28	136.8	1.02
R13544	51238.5568	–7.531	1.87	1.94	1.99	131.7	0.97
R13622	51250.4931	–7.761	1.87	1.94	2.04	122.3	0.95
R13741	51304.5682	–7.592	1.88	1.93	1.99	131.1	0.96
R13795	51316.3680	–7.629	1.88	1.95	2.00	126.4	0.97
R13799	51316.4734	–7.415	1.83	1.90	1.94	126.4	0.98
R13849	51323.3312	–8.020	1.89	2.04	2.00	128.7	1.02
R13851	51323.3469	–8.040	1.89	2.04	2.00	132.8	1.02
R13853	51323.3652	–8.020	1.89	2.04	2.00	129.9	1.02
R13855	51323.3851	–8.095	1.89	2.04	2.00	128.7	1.02
R13857	51323.4095	–8.045	1.89	2.04	2.00	129.3	1.02
R13859	51323.4402	–8.078	1.89	2.04	2.00	128.7	1.02
R13868	51325.3803	–7.913	1.90	2.05	1.95	127.5	1.05
R13920	51328.4117	–7.700	1.79	2.05	1.93	136.9	1.06
R13922	51328.4401	–7.790	1.81	2.05	1.94	139.2	1.05
R14118	51378.5441	–7.170	1.83	1.91	1.90	142.7	1.01
R14137	51379.4291	–7.501	1.86	1.94	1.92	119.3	1.01
R14276	51391.4448	–7.260	1.78	1.98	1.87	110.0	1.06
R14438	51401.3442	–7.992	1.85	2.01	1.88	138.2	1.07
R14477	51410.3629	–8.344	1.96	2.06	1.96	119.9	1.05
R14787	51433.3458	–8.124	1.95	2.00	2.00	104.1	1.00
R15597	51580.6094	–10.00	2.11	2.31	2.13	131.0	1.08
R15740	51602.4666	–10.35	2.19	2.24	2.30	107.5	0.97
R15898	51643.4587	–10.65	2.19	2.38	2.25	126.4	1.05
R15973	51656.3361	–10.60	2.24	2.32	2.31	117.0	1.00
R16003	51661.4248	–10.77	2.25	2.32	2.33	108.2	0.99
R16079	51669.3846	–10.13	2.19	2.28	2.26	114.1	1.01
R16137	51678.3676	–10.76	2.25	2.32	2.35	113.5	0.98
R16148	51679.3875	–10.72	2.25	2.32	2.33	117.6	0.99
R16150	51679.4007	–10.73	2.25	2.32	2.34	117.6	0.99
R16153	51679.4206	–10.79	2.25	2.33	2.34	118.2	0.99
R16154	51679.4386	–10.88	2.26	2.34	2.35	119.3	0.99
R16167	51680.3668	–10.61	2.25	2.31	2.31	118.8	0.99
R16195	51681.4057	–10.51	2.24	2.29	2.29	118.8	1.00
R16505	51714.3660	–11.01	2.26	2.40	2.34	117.6	1.02
HR1349	51924.5409	–15.04	2.78	2.93	2.90	108.0	1.01
HR1396	51936.5148	–14.57	2.75	2.90	2.89	97.28	1.00
HR1417	51938.5012	–14.74	2.72	2.92	2.87	84.73	1.02
HR1613	51959.5535	–14.16	2.65	2.89	2.74	81.30	1.06
HR1852	52005.3418	–15.23	2.83	3.01	2.93	68.74	1.03
HR1951	52027.4415	–15.57	2.86	2.99	—	97.30	—
HR1966	52029.3652	–15.70	2.87	3.01	—	82.44	—
HR2058	52038.5645	–15.76	2.85	—	—	109.8	—
CCD1639	52322.6262	–16.43	3.01	3.20	2.95	91.44	1.08
CCD1640	52322.6737	–17.24	3.03	3.30	2.92	95.55	1.13
HR3339	52343.4912	–17.38	3.04	3.15	3.14	80.53	1.00
HR3465	52352.5557	–16.57	3.08	3.24	—	85.42	—
HR3492	52362.3688	–18.37	—	—	—	72.17	—
HR3567	52366.3847	–18.62	3.24	—	—	64.43	—
HR3658	52373.4362	–19.50	3.31	3.48	3.44	75.60	1.01
HR3977	52417.4422	–17.38	2.95	3.35	—	75.60	—
HR5335	52657.5959	–20.00	3.46	3.46	3.54	79.48	0.97
HR5411	52683.5671	–21.27	3.56	3.63	3.60	56.41	1.01
HR5431	52684.4712	–21.17	3.62	3.67	3.64	56.19	1.00
HR5434	52684.5418	–20.70	3.57	3.60	3.59	53.67	1.00
HR5481	52687.4981	–20.72	3.52	—	—	—	—
HR5484	52687.5881	–20.76	—	—	—	—	—
HR5495	52688.4042	–21.31	—	3.71	—	—	—
HR5524	52692.4424	–20.87	3.41	3.62	3.38	94.10	1.07
HR5537	52693.4215	–21.70	3.49	3.74	3.48	94.33	1.07

Table 2. – continued

File	HJD –2400000	$W_{H\alpha}$ [Å]	I_c	I_V	I_R	$\Delta\nu_p$ [km s ^{–1}]	V/R
HR5757	52720.3170	–20.75	3.41	3.54	3.52	91.13	1.01
HR5793	52721.4772	–20.78	3.50	—	—	79.56	—
HR5816	52722.5142	–21.69	3.58	3.75	3.62	86.56	1.04
HR5836	52723.4036	–20.56	3.27	3.33	—	76.51	—
HR5837	52723.4325	–21.07	3.49	3.62	3.54	88.62	1.02
HR5864	52724.4549	–20.74	3.49	3.66	3.52	96.38	1.04
HR5926	52727.4657	–21.50	3.49	3.63	3.53	84.51	1.03
md0412	52734.7316	–20.51	3.39	3.37	3.43	64.20	0.984
md1118	52741.9524	–19.92	3.33	3.47	3.36	63.89	1.032
md1221	52742.6241	–20.37	3.38	3.53	3.42	60.96	1.032
md1222	52742.6307	–20.47	3.37	3.53	3.45	60.37	1.024
md1421	52744.8238	–20.44	3.42	3.56	3.45	52.75	1.032
md1422	52744.3828	–19.89	3.39	3.51	3.41	53.34	1.030
md1426	52744.8590	–20.06	3.40	3.52	3.43	53.34	1.026
md2111	52751.7782	–19.71	3.21	3.54	3.25	114.8	1.087
md2112	52751.7863	–19.81	3.22	3.55	3.26	115.5	1.091
md2114	52751.7979	–19.83	3.23	3.55	3.25	115.5	1.09
md2115	52751.8014	–19.78	3.21	3.54	3.26	114.9	1.088
md2229	52752.5113	–19.79	3.23	3.53	3.27	113.1	1.078
md2429	52754.8454	–19.97	3.20	3.53	3.30	113.1	1.07
md2430	52754.8493	–20.09	3.19	3.53	3.30	111.3	1.07
md2431	52754.8534	–20.21	3.21	3.54	3.32	113.7	1.07
md2432	52754.8576	–19.96	3.19	3.52	3.32	113.1	1.062
md2433	52754.8600	–20.08	3.22	3.56	3.29	111.9	1.081
md2434	52754.8624	–19.93	3.20	3.54	3.29	111.4	1.077
md2435	52754.8644	–20.12	3.21	3.54	3.30	111.9	1.07
md2436	52754.8680	–19.98	3.20	3.52	3.31	111.4	1.063
md2437	52754.8699	–19.97	3.20	3.54	3.31	110.8	1.068
md2438	52754.8733	–19.89	3.22	3.53	3.30	112.5	1.07

Table 4. Measured parameters of Si II 6347, Si II 6371, He I 6678, and Fe II 6456 lines.

File	HJD –2400000	Si II 6347 Å		Si II 6371 Å		He I 6678 Å		Fe II 6456 Å	
		$W[\text{Å}]$	I_c	$W[\text{Å}]$	I_c	$W[\text{Å}]$	I_c	$W[\text{Å}]$	I_c
R00311	48813.4315	0.04	0.970	0.001	0.981	0.172	0.971	–0.166	1.019
R00685	48883.50105	0.11	0.957	0.007	0.983	0.150	0.978	–0.089	1.010
R00743	48893.2294	0.13	0.953	0.077	0.974	0.206	0.970	–0.052	1.007
R00940	49018.5747	—	—	—	—	0.166	0.977	–0.165	1.015
R01270	49045.4875	0.14	0.969	0.130	0.976	0.201	0.967	–0.102	1.006
R01303	49066.4515	0.14	0.964	0.131	0.972	0.197	0.964	–0.044	1.001
R01381	49079.5350	0.13	0.964	0.112	0.972	0.213	0.965	–0.074	1.005
R01442	49081.4162	0.12	0.970	0.034	0.983	0.204	0.963	–0.162	1.012
R01448	49081.4524	0.14	0.961	0.083	0.981	0.205	0.953	–0.048	0.999
R01465	49088.3750	0.08	0.976	—	—	0.203	0.957	–0.098	1.008
R01515	49092.4614	0.07	0.972	—	—	0.202	0.960	–0.074	1.007
R01565	49102.3385	0.09	0.973	—	—	0.170	0.968	–0.068	1.003
R01566	49102.3636	0.07	0.977	—	—	0.161	0.969	–0.096	1.004
R01568	49102.3818	0.07	0.977	—	—	0.191	0.966	–0.103	1.009
R01697	49116.4731	0.12	0.957	0.102	0.979	0.209	0.955	—	—
R01740	49119.5657	0.08	0.971	0.061	0.978	0.207	0.964	—	—
R01839	49133.3452	0.13	0.966	0.137	0.964	0.162	0.975	—	—
R01849	49133.4032	0.13	0.957	0.054	0.978	0.157	0.967	—	—
R03466	49310.5844	0.08	—	0.026	—	0.182	—	–0.155	—
R03467	49310.6279	0.13	—	0.038	—	0.164	—	–0.112	—
R03601	49350.6331	0.08	0.974	0.095	0.978	0.164	0.969	–0.171	1.015
R03848	49403.6115	0.08	0.975	0.078	0.982	0.136	0.973	–0.116	1.009
R04243	49463.3294	0.08	0.966	0.074	0.974	0.168	0.967	–0.143	1.011
R04249	49463.3564	0.09	0.963	0.074	0.975	0.175	0.965	–0.098	1.008
R04261	49463.4929	0.09	0.966	0.089	0.978	0.160	0.968	–0.128	1.014
R04274	49463.5259	0.11	0.966	0.093	0.975	0.175	0.966	–0.086	1.009
R04406	49466.3311	0.09	0.970	0.081	0.979	0.171	0.972	–0.119	1.011
R04407	49466.3459	0.10	0.965	0.077	0.976	0.172	0.969	–0.074	1.010
R04427	49466.3994	0.10	0.970	0.078	0.978	0.127	0.971	–0.138	1.017
R04433	49466.4142	0.10	0.966	0.072	0.981	0.167	0.971	–0.079	1.011
R04445	49466.5338	0.09	0.963	0.074	0.980	0.162	0.969	–0.133	1.011
R04446	49466.5492	0.09	0.964	0.079	0.976	0.162	0.967	–0.076	1.010
R04462	49466.6149	0.09	0.962	0.080	0.973	0.167	0.965	–0.131	1.011
R04469	49467.3034	0.10	0.964	0.077	0.976	0.185	0.964	–0.076	1.007
R04484	49467.3497	0.10	0.963	0.082	0.977	0.171	0.969	–0.130	1.013
R04496	49467.4651	0.11	0.967	0.079	0.979	0.174	0.968	–0.083	1.010
R04515	49467.5566	0.11	0.963	0.082	0.976	0.182	0.969	–0.138	1.011
R07348	49702.6550	0.09	0.982	0.069	0.984	0.215	0.969	–0.145	1.011
R08124	49853.4086	0.09	0.971	0.074	0.981	0.188	0.964	–0.104	1.007
R08126	49853.4793	0.09	0.972	0.070	0.979	0.169	0.968	–0.031	1.001
R08190	49862.3759	0.09	0.968	0.085	0.976	0.191	0.967	–0.070	1.010
R08191	49862.3842	0.10	0.975	0.092	0.974	0.194	0.967	–0.033	1.003
R08551	49918.3372	0.09	0.957	0.084	0.970	0.205	0.964	–0.024	1.008
R08739	49930.3387	0.09	0.966	0.098	0.974	0.174	0.971	—	—
R09690	50080.6261	0.12	0.970	0.082	0.980	0.172	0.966	–0.071	1.006
R09862	50104.7034	0.11	0.972	0.088	0.979	0.172	0.970	—	—
R10089	50140.5900	0.10	0.971	0.091	0.979	0.173	0.969	—	—
R10245	50158.5779	0.10	0.976	0.080	0.982	0.183	0.966	—	—
R10268	50159.4882	0.08	0.963	0.122	0.976	0.187	0.966	—	—
R10285	50160.4201	0.09	0.967	0.097	0.978	0.187	0.972	—	—
R10562	50193.4706	0.10	0.975	0.125	0.972	0.182	0.966	–0.056	1.004
R10972	50249.4667	0.09	0.969	0.079	0.975	0.161	0.968	—	—
R10995	50251.3830	0.11	0.958	0.146	0.963	0.186	0.974	—	—
R11509	50316.3418	0.11	0.960	0.086	0.982	0.168	0.963	—	—
R12257	50448.6371	0.09	0.973	0.081	0.981	0.163	0.970	—	—
R12528	50506.5231	0.09	0.970	0.099	0.976	0.178	0.967	—	—
R12619	50509.5290	0.10	0.970	0.071	0.981	0.184	0.967	—	—
R12743	50518.4640	0.10	0.967	0.098	0.975	0.179	0.966	—	—

Table 4. – continued

File	HJD –2400000	Si II 6347 Å		Si II 6371 Å		He I 6678 Å		Fe II 6456 Å	
		W[Å]	I_c	W[Å]	I_c	W[Å]	I_c	W[Å]	I_c
R13044	50583.4009	0.09	0.969	0.085	0.974	0.181	0.965	—	—
R13544	51238.5568	0.13	0.978	0.043	0.988	0.120	0.978	–0.105	0.978
R13622	51250.4931	0.03	0.986	0.106	0.984	0.122	0.976	–0.118	0.976
R13795	51316.3680	0.15	0.975	0.076	0.977	0.164	0.977	0.0000	1.021
R13799	51316.4734	0.09	0.954	—	—	0.208	0.960	–0.079	1.021
R13842	51322.4657	0.09	0.984	0.050	0.983	0.152	0.971	—	—
R13849	51323.3312	0.10	0.989	0.043	0.988	0.144	0.975	–0.037	0.998
R13851	51323.3469	0.10	0.981	0.033	0.995	0.131	0.974	–0.133	1.010
R13853	51323.3652	0.07	0.969	0.039	0.988	0.151	0.974	–0.135	1.008
R13855	51323.3851	0.07	0.973	0.063	0.981	0.177	0.966	–0.175	1.014
R13857	51323.4095	0.07	0.972	0.042	0.991	0.165	0.968	–0.182	1.013
R13859	51323.4402	0.07	0.974	0.052	0.984	0.153	0.969	–0.147	1.009
R13868	51325.3803	0.08	0.969	0.066	0.979	0.144	0.973	–0.133	1.002
R13920	51328.4117	0.08	0.963	0.080	0.968	0.147	0.972	—	—
R13922	51328.4401	0.08	0.962	0.093	0.972	0.148	0.973	—	—
R14118	51378.5441	0.05	0.966	0.062	0.979	0.165	0.974	—	—
R14137	51379.4291	0.06	0.969	0.052	0.983	0.187	0.974	—	—
R14276	51391.4448	0.06	0.970	0.058	0.978	0.182	0.972	—	—
R14438	51401.3442	—	—	—	—	0.114	0.980	—	—
R14477	51410.3629	0.05	0.974	0.049	0.986	0.148	0.975	—	—
R14787	51433.3458	0.07	0.965	0.083	0.977	0.158	0.972	—	—
R15597	51580.6094	0.06	0.975	—	—	0.133	0.973	–0.071	1.001
R15740	51602.4666	0.06	0.983	0.030	0.990	0.138	0.975	–0.181	1.011
R15898	51643.4587	0.04	0.983	—	—	0.112	0.977	–0.102	1.001
R15973	51656.3361	0.06	0.974	0.088	0.974	0.134	0.975	–0.100	0.996
R16003	51661.4248	0.05	0.978	0.039	0.986	0.130	0.974	–0.068	0.997
R16079	51669.3846	0.06	0.969	0.036	0.983	0.132	0.976	–0.127	1.011
R16137	51678.3676	0.05	0.983	0.026	0.990	0.139	0.976	–0.080	1.004
R16148	51679.3875	0.04	0.976	0.039	0.988	0.152	0.975	–0.213	1.010
R16150	51679.4007	0.05	0.978	0.035	0.989	0.127	0.979	–0.159	1.009
R16153	51679.4206	0.05	0.979	0.047	0.984	0.140	0.974	–0.223	1.017
R16154	51679.4386	0.05	0.975	0.038	0.944	0.142	0.976	–0.228	1.019
R16167	51680.3668	0.04	0.975	0.050	0.984	0.133	0.972	–0.211	1.015
R16195	51681.4057	0.05	0.974	0.042	0.978	0.140	0.978	–0.207	1.015
R16505	51714.3660	0.07	0.971	0.036	0.985	0.140	0.975	–0.085	1.002
HR1349	51924.5409	0.10	0.974	0.052	0.983	0.170	0.967	–0.110	0.992
HR1396	51936.5148	0.14	0.959	—	—	0.114	0.977	–0.253	1.009
HR1417	51938.5012	0.12	0.966	—	—	0.194	0.966	–0.217	1.012
HR1951	52027.4415	0.10	0.966	—	—	0.135	0.972	–0.219	1.011
HR1966	52029.3652	0.14	0.949	—	—	0.134	0.976	–0.113	1.001
HR2058	52038.5645	0.11	0.957	—	—	0.178	0.974	–0.153	1.004
CCD1639	52322.6262	0.08	0.966	—	—	0.158	0.969	–0.213	1.008
CCD1640	52322.6737	0.05	0.972	—	—	0.165	0.974	–0.245	1.014
HR3339	52343.4912	0.17	0.961	—	—	0.150	0.965	–0.480	1.039
HR3465	52352.5557	0.15	0.951	—	—	0.153	0.968	–0.629	1.052
HR3492	52362.3688	0.14	0.962	—	—	0.144	0.972	–0.314	1.018
HR3567	52366.3847	0.08	0.972	—	—	0.122	0.968	–0.292	1.016
HR3658	52373.4362	0.08	0.970	—	—	0.129	0.975	–0.365	1.025
HR3977	52417.4422	0.17	0.950	—	—	0.139	0.974	–0.513	1.037
HR5335	52657.5959	0.05	0.981	—	—	0.156	0.972	–0.330	1.020
HR5411	52683.5671	0.09	0.977	—	—	0.140	0.954	–0.279	1.015
HR5431	52684.4712	0.06	0.976	—	—	0.151	0.969	–0.341	1.023
HR5434	52684.5418	0.06	0.974	—	—	0.134	0.974	–0.380	1.028
HR5481	52687.4981	0.07	0.977	—	—	0.139	0.975	–0.383	1.026
HR5484	52687.5881	0.07	0.977	—	—	0.130	0.975	–0.377	1.023
HR5495	52688.4042	0.05	0.979	—	—	0.133	0.969	–0.373	1.024
HR5524	52692.4424	0.06	0.978	—	—	0.151	0.972	–0.391	1.024
HR5537	52693.4215	0.05	0.978	—	—	0.132	0.970	–0.389	1.022

Table 4. – continued

File	HJD –2400000	Si II 6347 Å		Si II 6371 Å		He I 6678 Å		Fe II 6456 Å	
		$W[\text{Å}]$	I_c	$W[\text{Å}]$	I_c	$W[\text{Å}]$	I_c	$W[\text{Å}]$	I_c
HR5757	52720.317	—	—	0.04	0.99	0.184	0.967	–0.486	1.033
HR5793	52721.4772	—	—	—	—	0.122	0.968	–0.323	1.020
HR5816	52722.5142	—	—	—	—	0.080	0.976	–0.481	1.036
HR5836	52723.4036	0.05	0.977	—	—	0.136	0.972	–0.428	1.028
HR5837	52723.4325	—	—	—	—	0.152	0.969	–0.490	1.036
HR5864	52724.4549	—	—	—	—	0.101	0.974	–0.563	1.037
HR5926	52727.4657	0.05	0.971	—	—	0.256	0.954	–0.380	1.022
md0412	52734.7316	0.063	0.970	—	—	0.178	0.965	–0.402	1.025
md1118	52741.9524	0.030	0.980	—	—	0.150	0.971	–0.385	1.025
md1221	52742.6241	0.067	0.973	—	—	0.145	0.973	–0.415	1.025
md1222	52742.6307	0.069	0.964	—	—	0.166	0.969	–0.468	1.036
md1421	52744.8203	0.076	0.968	—	—	0.134	0.979	–0.391	1.030
md1422	52744.8238	0.020	0.981	—	—	0.142	0.969	–0.393	1.019
md1426	52744.8590	0.030	0.979	—	—	0.145	0.973	–0.436	1.028
md2111	52751.7782	0.062	0.972	—	—	0.141	0.977	–0.380	1.028
md2112	52751.7863	0.066	0.975	—	—	0.158	0.968	–0.403	1.026
md2114	52751.7979	0.074	0.975	—	—	0.153	0.973	–0.400	1.024
md2115	52751.8014	0.026	0.974	—	—	0.161	0.977	–0.389	1.026
md2229	52752.5113	0.047	0.973	—	—	0.15	0.966	–0.415	1.022
md2429	52754.8454	0.07	0.977	—	—	0.157	0.971	–0.40	1.025
md2430	52754.8493	0.032	0.977	—	—	0.107	0.981	–0.45	1.025
md2431	52754.8534	0.053	0.973	—	—	0.133	0.977	–0.43	1.029
md2432	52754.8576	0.043	0.979	—	—	0.15	0.973	–0.405	1.023
md2433	52754.8600	0.049	0.97	—	—	0.147	0.97	–0.406	1.03
md2434	52754.8624	0.064	0.967	—	—	0.133	0.971	–0.429	1.019
md2435	52754.8644	0.058	0.977	—	—	0.175	0.97	–0.430	1.031
md2436	52754.8680	0.072	0.966	—	—	0.122	0.982	–0.4	1.028
md2437	52754.8699	0.072	0.971	—	—	0.135	0.971	–0.431	1.025
md2438	52754.8733	0.043	0.983	—	—	0.141	0.977	–0.428	1.026